Phonon interference control of atomic-scale metamirrors, meta-absorbers, and heat transfer through crystal interfaces

Yu. A. Kosevich,[1,2,*] L. G. Potyomina,[3] A. N. Darinskii,[4,5] and I. A. Strelnikov[1]

[1]*Semenov Institute of Chemical Physics of Russian Academy of Sciences, 4 Kosygin str., 119991 Moscow, Russia*

[2]*Plekhanov Russian University of Economics, 36 Stremyanny per., 117997 Moscow, Russia*

[3]*Educational-Scientific Institute of Physical Engineering, National Technical University "Kharkiv Polytechnic Institute", 2 Kirpichova str., 61002 Kharkiv, Ukraine*

[4]*Institute of Crystallography FSRC "Crystallography and Photonics", 59 Leninsky av., 119333 Moscow, Russia*

[5]*National University of Science and Technology "MISiS", 4 Leninsky av., 119049 Moscow, Russia*

(Received 11 December 2017; revised manuscript received 18 February 2018; published 30 March 2018)

The paper theoretically studies the possibility of using the effects of phonon interference between paths through different interatomic bonds for the control of phonon heat transfer through internal crystal interfaces and for the design of phonon metamirrors and meta-absorbers. These metamirrors and meta-absorbers are considered to be defect nanolayers of atomic-scale thicknesses embedded in a crystal. Several analytically solvable three-dimensional lattice-dynamics models of the phonon metamirrors and meta-absorbers at the internal crystal planes are described. It is shown that due to destructive interference in the two or more phonon paths, the internal crystal planes, fully or partially filled with weakly bound or heavy-isotope defect atoms, can completely reflect or completely absorb phonons at the transmission antiresonances, whose wavelengths are larger than the effective thickness of the metamirror or meta-absorber. Due to cooperative superradiant effect, the spectral widths of the two-path interference antiresonances for the plane waves are given by the square of partial filling fraction in the defect crystal plane. Our analysis reveals that the presence of two or more phonon paths plays the dominant role in the emergence of the transmission antiresonances in phonon scattering at the defect crystal planes and in reduction of the thermal interface conductance in comparison with the Fano-resonance concept. We study analytically phonon transmission through internal crystal plane in a model cubic lattice of Si-like atoms, partially filled with Ge-like defect atoms. Such a plane can serve as interference phonon metamirror with the transmission antiresonances in the vicinities of eigenmode frequencies of Ge-like defect atoms in the terahertz frequency range. We predict the extraordinary phonon transmission induced by the two-path constructive interference of the lattice waves in resonance with the vibrations of rare host atoms, periodically distributed in the crystal plane almost completely filled with heavy-isotope defects. We show that the phonon-interference-induced transparency can be produced by the defect nanolayer with the non-nearest-neighbor interactions, filled with two types of isotopes with relatively small difference in masses or binding force constants. In this case, relatively broad transmission antiresonance is accompanied by the narrow transmission peak close to the antiresonance frequency. We describe the softening of the flexural surface acoustic wave, localized at the embedded defect nanolayer, caused by negative surface stress in the layer. The surface wave softening results in spatially periodic static bending deformation of the embedded nanolayer with the definite wave number. The latter effect is estimated for graphene monolayer embedded in a strained matrix of polyethylene. We analyze the effect of nonlinearity in the dynamics of defect atoms on the one- and two-path phonon interference and show that the interference transmission resonances and antiresonances are shifted in frequencies but not completely suppressed by rather strong anharmonicity of interatomic bonds. The reduction of the Kapitza thermal interface conductance caused by the destructive phonon interference in a defect monolayer is described. We show that the additional relatively weak non-nearest-neighbor interactions through the defect crystal plane filled with heavy isotopes substantially reduces the interface thermal conductance, and this effect is stronger in the three-dimensional system than in the quasi-one-dimensional systems studied previously.

DOI: 10.1103/PhysRevB.97.094117

I. INTRODUCTION

The Kapitza thermal interface resistance was discovered at a solid-liquid helium contact in 1941 [1] and later at solid-solid interfaces [2]. It results in the enhancement of the total heat resistance, which is a sum of the bulk thermal resistance and the boundary thermal one. The studies of the thermal interface resistance and thermal interface conductance are in the focus of both experimental and theoretical studies since then and they have become very active in the last years because it was realized that the thermal interface conductance is especially important in nanoscale systems with relatively high ratio of surface and bulk atoms [3–8], in nanostructures such as superlattices, nanowires, and nanoribbons [9–16], and in metamaterials [17]. During the last decade, phonon transport across interfaces

*Corresponding author: yukosevich@gmail.com

between crystals has been studied in a considerable number of papers with the use of molecular dynamics simulations (see, e.g., Refs. [18–30]). The thermal transport has also been investigated using the nonequilibrium Green function method [31,32]. However, numerical computations do not undermine the importance of analytically solvable models. Such models permit one to highlight visually the physical effects controlling the phonon transport that can be verified subsequently in more realistic models with the help of numerical methods.

The first modeling of the thermal interface conductance of a solid-liquid helium interface has been carried out in Ref. [33] (see also [34]). The theory is based on the idea that the phonon transmission is equivalent to the transmission of ordinary dispersionless acoustic waves. In addition, it was assumed in this model that the interface is perfectly flat and the contact is perfectly rigid. The transmission coefficient is obtained by solving the acoustic transmission/reflection problem at the interface between two media with very different acoustic properties and, respectively, with strongly mismatched acoustic impedances [the acoustic mismatch model (AMM)]. The AMM was later developed and applied to various cases with the account of the specific features, which were not taken into account initially, such as the contribution of transverse phonons in solids, anisotropy of elastic properties, and phonon focusing (see, e.g, Refs. [35–42]). The influence of the dispersion of group velocity on the transmission of phonons across the solid-solid interfaces was investigated within the frame of the lattice dynamics in one-dimensional (1D) [43–46], two-dimensional (2D) [47], and three-dimensional (3D) [48–51] systems. It is worth noting that a special model, commonly referred to as the diffuse mismatch model, has been developed in order to describe the phonon transmission under the condition of strong surface diffuse scattering [52–55].

The influence of anharmonic effects on the phonon transmission was studied within the frame of lattice dynamics approach [56,57], as well as on the basis of the continuum description of phonon dynamics [58]. For example, according to [58], the interface eigenmodes, which can be present at the interface between two crystals with strongly different elastic properties and phonon spectra, can substantially affect the phonon transmission through the interface. Namely, the acoustic phonons, incident from the crystal with higher phonon frequencies, can enter the other crystal at the subharmonics (one-half or one-third harmonics) of the incident phonon frequency. While the acoustic phonons, incident from the crystal with lower phonon frequencies, can enter the other crystal at the multiple (second or third) harmonics (see also [59]). These processes can significantly contribute to the thermal interface conductance and to the *nonreciprocity* of the heat transfer through the nonlinear and strongly mismatched (asymmetric) interfaces [58].

When two solids are brought into contact by pressing them to each other, due to surface roughness the contact actually occurs only within multiple isolated very narrow (pointlike) areas. The theory of the ballistic phonon transport in such contacts and the relevant experimental results are comprehensively reviewed in [60].

An interesting situation can occur when a homogeneous crystal is broken into two parts by an ultrathin interface layer. At first glance, such a boundary should only weakly perturb the propagation of ballistic phonons and the thermal boundary resistance will be negligible. But, the analysis reveals that this is not necessarily the case. In Refs. [58,61–66] the phonon transmission across the interface between two solids, stipulated by vibrational eigenmodes in the defect layer, was investigated. In these works, the bulk phonon characteristics are described with the linear theory of elasticity and low-frequency dynamical properties of the interface layer are described with the use of macroscopic "capillary parameters," which take into account the interaction of bulk acoustic waves with the ultrathin interface layer via the additional boundary (interface) conditions for the elastic stresses and displacements (see a review paper [66]). It was shown that the transmission of obliquely incident long-wavelength bulk phonon can drop to zero through the ultrathin layer inserted into a homogeneous crystal [61,62,67–70]. This effect occurs either because the transverse bulk wave cannot propagate along the ultrathin layer in which the local speed of the acoustic wave of corresponding polarization is different from the bulk one [61,62] or because of resonance excitation of the leaky interface wave caused by the presence of the ultrathin defect layer embedded in a crystal [67–71]. Thus, it appears that under certain conditions an ultrathin interface layer with atomic-scale thickness can play the role of a perfect mirror for bulk phonons.

Destructive interference effects in 2D (planar) defect for acoustic phonons (elastic waves) were first described in Ref. [66], in which the resonance of total reflection (transmission antiresonance) and the resonance of total absorption of long acoustic waves in a crystal with an embedded ultrathin defect layer were revealed. These resonances were related with the destructive interference between the two possible phonon paths: through the nearest-neighbor defect-host interatomic bonds and through the non-nearest-neighbor bonds which couple directly the host crystal planes adjacent to the defect atomic plane. The later works [72,73] considered within the frame of lattice dynamics the phonon multichannel scattering by the defect atoms inserted in the quasi-1D atomic chain, which effectively models normal incidence of bulk phonons on 2D defect in 3D crystal. The existence of several propagation paths results in the interference of phonons, similar to the celebrated *two-slit interference of light*. It was shown that the destructive interference reduces phonon transmission through the defect layer up to zero at certain frequencies (transmission antiresonances), which are determined by the frequencies of the defect vibrational eigenmodes. The occurrence of the phonon-interference-induced transmission antiresonances, described in [66,72], was confirmed by numerical studies within the frame of molecular dynamics of the atomic-scale metamaterial made of the internal crystal plane, fully or partially filled with heavy-isotope atomic defects [74–77]. Essentially, the transmission spectra obtained in [74,75,77] were reproduced by the relevant quasi-1D models proposed in [72]. We emphasize that the two-path destructive phonon interference yielding the vanishing transmission is similar to the total cancellation of the photon output due to the coalescence of the two single photons which interfere destructively upon propagation through two different photon paths [78–82].

We also emphasize that the presence of two or more phonon paths is decisive in the emergence of the transmission antiresonances in phonon scattering at the 2D defect crystal plane, which cannot be properly described by the Fano

resonance. This can be confirmed by studying phonon transmission through the atomic chain, which contains an embedded weakly bound or heavy-isotope impurity atom, when the transmission spectral line shows either single resonance transmission peak [see Figs. 8(a) and 9(a) below] or monotonous decay with frequency [see lines 2 in Figs. 5(d) and 5(e) and line 3 in Fig. 17(c) below], without any zero-transmission dip. Similar features have the phonon transmission spectra through the internal crystal plane (planar defect) fully filled with weakly bound or heavy-isotope impurity atoms (see Sec. V below). The presence of the weakly bound or heavy-isotope defects embedded in an atomic chain or in a crystal plane fully satisfies the Fano-resonance condition [83] of the local state resonating with the continuum of phonon eigenstates in the system, but zero-transmission antiresonances and total absorption of long acoustic waves do not occur because of the absence of the *two different phonon paths* in the system [64,66,72]. The line shape of the anomalous interface absorption, which is caused by the two-path phonon interference under the double-resonance conditions [see Fig. 4(a) below] also does not have the asymmetric Lorentzian shape, which is usually related with the shape of the absorption line produced by the Fano resonance [83]. The transmission and reflection spectra, presented in Figs. 9(a) and 9(b) below, show that the *additional phonon path* through the non-nearest-neighbor interatomic bonds across the defect layer can drastically change phonon transmittance of the system with almost no change in the eigenfrequency and polarization of the local vibrational mode resonating with the continuum of phonon eigenstates in the system, in contrast to the concept of the Fano resonance. The transmission peak produced by the weakly bound impurity atoms, like the peaks shown in Figs. 8(a) and 9(a) below, can be considered as phonon analog of the Fabry-Pérot resonance in optics, which occurs due to constructive interference and requires only a *single path* for photons or phonons. These examples of the atomic-scale defects, inserted in an atomic chain or in a crystal plane, clearly demonstrate the two-path or multipath destructive-interference nature of the considered antiresonances in the phonon transmission spectra (see also [74,75]).

This paper studies the phonon resonance transmission, reflection, and anomalous absorption in 3D lattices, caused by the two-path and multipath phonon interference in embedded impurity monolayers. Actual structures conforming these models can be created by complete filling of the internal crystal plane with atomic impurities with long-range interatomic bonds or by partial filling of a crystal plane with heavy-isotope or weakly bound atomic impurities. Our main interest is focused on the acoustic phonon transmission and absorption features, which are directly related with the two-path and multipath phonon interference and which do not show up in the case of the one-path constructive phonon interference which results in the Fabry-Pérot–type resonance transmission enhancement [25,64,65].

We demonstrate that the crystal plane, partially filled with the atomic impurities, can become a strong obstacle for bulk phonons, which means that within certain frequency ranges the defect layers of atomic-scale thicknesses are able to operate as perfect phonon metamirrors or meta-absorbers in realistic 3D crystal structures. We show the occurrence of two transmission antiresonances at the defect plane filled with two types of impurities and long-range interatomic bonds, produced by three different phonon paths through such two-dimensional defect. We show that due to the cooperative superradiant effect, the spectral widths of the two-path interference antiresonances for the plane waves are given by the square of surface density or partial filling fraction of atomic defects in the crystal plane.

We describe the *anomalous interface absorption* with the total nontransmission and nonreflection of the incident phonon at the double-resonant nanolayer with two equal frequencies of the defects eigenmodes and two phonon paths through the defect plane. We predict the *extraordinary phonon transmission* induced by the two-path constructive interference of lattice waves interacting with resonance oscillations of rare host atoms, periodically distributed in the crystal plane almost fully filled with heavy isotopes. We show that the *phonon-interference-induced transparency* can be produced by the defect monolayer with the non-nearest-neighbor interactions, filled with two types of isotopes with relatively small difference in vibrational eigenfrequencies. In this case, relatively broad transmission antiresonance is accompanied by the narrow transmission peak close to the antiresonance frequency.

We describe within the analytical model the change from the total transmission to total reflection of the grazing-incident waves at the defect monolayer, the anomalous resonance surface absorption, when 50% of the energy of the oblique-incident long acoustic wave is absorbed at the monolayer defect, and the softening of the flexural surface acoustic wave, localized at the monolayer defect plane, caused by negative (compressive) surface stress g_{xx} and finite bending stiffness D_s of the 2D elastic layer. Softening of the flexural surface acoustic wave results in spatially periodic static bending deformation (modulation) with the definite wave number k_{x0} of the nanolayer, embedded in a strained matrix. This effect can be triggered, e.g., by the compression of the solid along the x axis, which results in the compressive strain and negative surface stress g_{xx} in the embedded 2D elastic layer. We estimate the necessary compressive strain ϵ_{xx}, in fact very small, and the resulting modulation wavelength $\lambda_0 = 2\pi/k_{x0}$, in fact rather big, for the *graphene monolayer*, embedded in a strained matrix of low-density polyethylene: $\epsilon_{xx} = -2.5 \times 10^{-3}$, $\lambda_0 = 48$ Å.

We analyze the effect of nonlinearity on the one-path and two-path phonon interference and show that the interference transmission antiresonances and resonances are shifted in frequencies but are not fully suppressed by rather strong anharmonicity of interatomic bonds. We analyze how destructive phonon interference in a defect monolayer reduces the Kapitza thermal interface conductance and show that, counterintuitively, the additional relatively weak non-nearest-neighbor coupling through the defect crystal plane with heavy-isotope atoms substantially decreases the interface thermal conductance, and that this effect is more pronounced in 3D system than in the quasi-1D systems, studied previously [77]. The latter occurs because of higher density of phonon states in the high-frequency domain in the 3D system, in which the transmission is most strongly suppressed by the additional phonon paths.

The paper is organized as follows. In Sec. II we describe a general model with three types of the atoms with the mass

and interatomic bond defects, distributed along the crystal plane in a cubic lattice. This model predicts the existence of two transmission antiresonances provided that there are three paths for phonons to cross the atomic-scale defect layer. In Sec. III we describe the anomalous total interface energy absorption in phonon scattering at the double-resonant internal monolayer with two equal frequencies of the defect eigenmodes and with two phonon paths through the defect plane. In Sec. IV, phonon scattering at the crystal plane, 50% filled in the chessboard order by atoms with the mass and/or interatomic force constants defects, is investigated. Phonon-interference-induced transparency, produced by the defect monolayer with the non-nearest-neighbor interactions, filled with two types of isotopes with relatively small difference in masses or interatomic force constants, is described in this section. Here, we also describe the extraordinary phonon transmission induced by the two-path constructive interference of lattice waves interacting with resonance oscillations of rare host atoms, periodically distributed in the crystal plane almost completely filled with heavy-isotope defects. In Sec. V we describe phonon scattering at homogeneous embedded monolayer. Here, the appearance of the transmission antiresonance caused by the non-nearest-neighbor interactions through the defect crystal plane, completely filled with defect atoms, is described. We also describe here the change from the total transmission to total reflection of the grazing-incident waves at the monolayer defect, anomalous surface absorption of the incident long acoustic wave at the monolayer defect, and the softening of the flexural surface acoustic wave, localized at the monolayer defect plane, caused by the negative surface stress in the 2D elastic layer. In Sec. VI we describe the effects of nonlinearity in the dynamics of defect atoms on the two-path phonon interference. In Sec. VII we analyze how destructive phonon interference in a defect monolayer decreases the Kapitza thermal interface conductance. In the Conclusions we summarize the main results presented in the paper.

II. PHONON SCATTERING BY TRIPLE DEFECT LAYER

We consider the bcc lattice which fragment is shown in Fig. 1. The mass of host atoms (black circles) is m. There are three sorts of impurities with masses m_1 (crossed circles), m_1^* (gray circles), and m_2 (empty circles), respectively. The atom position is specified by three integers p_i, $i = 1,2,3$. The indices $p_{1,2}$ and p_3 are counted off, respectively, horizontally and vertically. It is expedient to ascribe even integers to cell sites and odd integers to cell centers.

Impurities m_1 lie in the plane $p_3 = 0$ at cell sites. We mark their positions by $(2n_1 + 2,2n_2,0)$ assuming that a pair (n_1,n_2) labels the corresponding column of cells (Fig. 1). Impurities m_1^* are labeled by $(2n_1,2n_2,0)$ since they are also at cell sites in the plane $n_3 = 0$. Impurities m_2 take positions $(2n_1 + 1,2n_2 + 1, \pm 1)$. Host atoms are indexed by triplets $(2n_1,2n_2,2n_3)$, where $n_3 \neq 0$, and $(2n_1 + 1,2n_2 + 1,2n_3 + 1)$, where $n_3 \neq 0, -1$. Summing up, the defect region comprises three atomic planes $p_3 = 0, \pm 1$ [the triple-layer (TL) model].

In our model, displacements of atoms are one component. We denote the displacement of an atom in position (p_1, p_2, p_3) by $u_{p_1}^{p_2,p_3}$. All three p_i in each triplet of indices occur to be either even or odd, i.e., either $p_i = 2n_i$ or $p_i = 2n_i + 1$ for $i = 1,2,3$. Below, when considering the propagation of phonons, for the sake of definiteness and consistency with the form of interatomic interactions, we assume that the displacement is always directed normally to the defect planes.

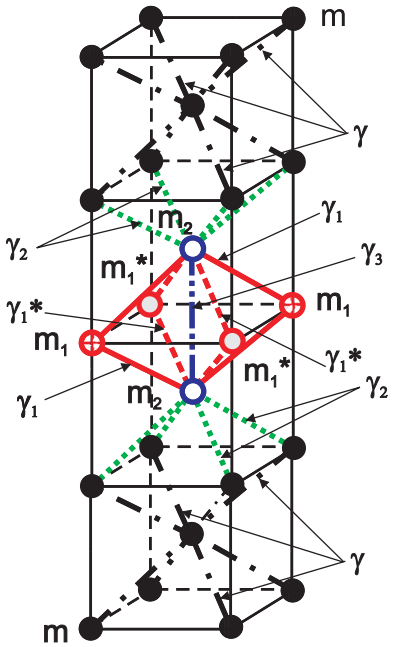

FIG. 1. General model. Lines interconnecting nodes indicate cell borders. Circles at the centers and sites of the cells are different sorts of atoms. Lines drawn between centers and sites as well as between two centers symbolize nearest-neighbor and next-to-nearest-neighbor bonds.

Basically, we take into account only the nearest-neighbor interaction, that is, the interaction between an atom at the cell center and its nearest eight neighbors at lattice nodes. The next-to-nearest-neighbor interaction is allowed for only between impurity atoms m_2 (see Fig. 1). The force constant γ characterizes the interaction between host atoms. The symbols γ_1 and γ_1^* stand for the force constants of nearest-neighbor interactions between impurities $m_1 \leftrightarrow m_2$ and $m_1^* \leftrightarrow m_2$, respectively. The constant of the next-to-nearest-neighbor interaction between impurities m_2 is denoted by γ_3.

The lattice Hamiltonian $H = E_{\rm kin} + U$ involves the kinetic energy $E_{\rm kin}$ and potential energy U of atoms:

$$E_{\rm kin} = \frac{1}{2}\left[m \sum_{p_i, |p_3| \geqslant 2} \left(\dot{u}_{p_1}^{p_2,p_3}\right)^2 + \sum_{m=1}^{2} \sum_{n_1,n_2} E_{n_1,n_2}^{(m)} \right], \qquad (1)$$

where in the first term the summation runs over the triplets of even integers $p_{1,2,3}$ and odd integers $p_{1,2,3}$, except for those with $p_3 = 0, \pm 1$:

$$\begin{aligned} E_{n_1,n_2}^{(1)} &= m_1 \left(\dot{u}_{2n_1+2}^{2n_2,0}\right)^2 + m_1^* \left(\dot{u}_{2n_1}^{2n_2,0}\right)^2, \\ E_{n_1,n_2}^{(2)} &= m_2 \left[\left(\dot{u}_{2n_1+1}^{2n_2+1,1}\right)^2 + \left(\dot{u}_{2n_1+1}^{2n_2+1,-1}\right)^2 \right]. \end{aligned} \qquad (2)$$

The parabolic potential energy is the following:

$$U = \frac{1}{2}\sum_{n_1,n_2}\left[\sum_{|n_3|\geqslant 2} U^{n_3}_{n_1n_2} + \sum_{m=1}^{5} U^{(m)}_{n_1n_2}\right], \tag{3}$$

where

$$\begin{aligned}
U^{n_3}_{n_1n_2} &= \gamma\sum_{\delta_i}\left(u^{2n_2,2n_3}_{2n_1} - u^{2n_2+\delta_2,2n_3+\delta_3}_{2n_1+\delta_1}\right)^2,\\
U^{(1)}_{n_1n_2} &= \gamma\sum_{\delta_i}\left(u^{2n_2,2\delta_3}_{2n_1} - u^{2n_2+\delta_2,3\delta_3}_{2n_1+\delta_1}\right)^2,\\
U^{(2)}_{n_1n_2} &= \gamma_1\sum_{\delta_i}\left(u^{2n_2,0}_{2n_1+2} - u^{2n_2+\delta_2,\delta_3}_{2n_1+2+\delta_1}\right)^2,\\
U^{(3)}_{n_1n_2} &= \gamma_1^*\sum_{\delta_i}\left(u^{2n_2,0}_{2n_1} - u^{2n_2+\delta_2,\delta_3}_{2n_1+\delta_1}\right)^2,\\
U^{(4)}_{n_1n_2} &= \gamma_2\sum_{\delta_i}\left(u^{2n_2,2\delta_3}_{2n_1} - u^{2n_2+\delta_2,\delta_3}_{2n_1+\delta_1}\right)^2,\\
U^{(5)}_{n_1n_2} &= \gamma_3\left(u^{2n_2+1,1}_{2n_1+1} - u^{2n_2+1,-1}_{2n_1+1}\right)^2.
\end{aligned} \tag{4}$$

The index δ_i at the summation symbol means that the summation is over eight combinations of $\delta_1,\delta_2,\delta_3 = \pm 1$.

In view of Eqs. (1)–(4), the equations of motion in the lattice dynamics can be represented in the following form:

$$m\ddot{u}^{p_2,p_3}_{p_1} = -\gamma\sum_{\delta_i} D^{\delta_2,\delta_3}_{\delta_1}, \quad |p_3| \geqslant 3 \tag{5}$$

where

$$D^{\delta_2,\delta_3}_{\delta_1} = u^{p_2,p_3}_{p_1} - u^{p_2+\delta_2,p_3+\delta_3}_{p_1+\delta_1}, \tag{6}$$

$p_{1,2,3}$ are triplets of even and odd integers;

$$m\ddot{u}^{2n_2,2\delta_3}_{2n_1} = -\sum_{\delta_{1,2}}\left[\gamma D^{\delta_2}_{\delta_1} + \gamma_2\tilde{D}^{\delta_2}_{\delta_1}\right], \tag{7}$$

where

$$\begin{aligned}
D^{\delta_2}_{\delta_1} &= u^{2n_2,2\delta_3}_{2n_1} - u^{2n_2+\delta_2,3\delta_3}_{2n_1+\delta_1},\\
\tilde{D}^{\delta_2}_{\delta_1} &= u^{2n_2,2\delta_3}_{2n_1} - u^{2n_2+\delta_2,\delta_3}_{2n_1+\delta_1}.
\end{aligned} \tag{8}$$

The index $\delta_{1,2}$ at the summation symbol implies the summation over four possible combinations of $\delta_1,\delta_2 = \pm 1$:

$$m_1\ddot{u}^{2n_2,0}_{2n_1+2} = -\gamma_1\sum_{\delta_i}\left(u^{2n_2,0}_{2n_1+2} - u^{2n_2+\delta_2,\delta_3}_{2n_1+2+\delta_1}\right), \tag{9}$$

$$m_1^*\ddot{u}^{2n_2,0}_{2n_1} = -\gamma_1^*\sum_{\delta_i}\left(u^{2n_2,0}_{2n_1} - u^{2n_2+\delta_2,\delta_3}_{2n_1+\delta_1}\right), \tag{10}$$

and

$$m_2\ddot{u}^{2n_2+1,\delta_3}_{2n_1+1} = \gamma_2\left[\sum_{\delta_{1,2}}\bar{D}^{\delta_2}_{\delta_1}\right] + \gamma_1\bar{D}' + \gamma_1^*\bar{D}^{*\prime} - \delta_3\gamma_3\bar{\bar{D}}, \tag{11}$$

where

$$\begin{aligned}
\bar{D}^{\delta_2}_{\delta_1} &= u^{2n_2+1+\delta_2,2\delta_3}_{2n_1+1+\delta_1} - u^{2n_2+1,\delta_3}_{2n_1+1},\\
\bar{D}' &= u^{2n_2+2,0}_{2n_1} + u^{2n_2,0}_{2n_1+2} - 2u^{2n_2+1,\delta_3}_{2n_1+1},\\
\bar{D}^{*\prime} &= u^{2n_2+2,0}_{2n_1+2} + u^{2n_2,0}_{2n_1} - 2u^{2n_2+1,\delta_3}_{2n_1+1},\\
\bar{\bar{D}} &= u^{2n_2+1,1}_{2n_1+1} - u^{2n_2+1,-1}_{2n_1+1}.
\end{aligned} \tag{12}$$

These equations describe, respectively, the vibrations of the host atoms in the planes $|p_3| \geqslant 3$ and $p_3 = \pm 2$ [Eqs. (5) and (8)], the vibrations of impurities in the plane $p_3 = 0$ [Eqs. (9) and (10)], and the vibrations of impurities in the planes $p_3 = \pm 1$ [Eq. (11)].

From Eq. (5), the bulk phonon spectrum in the host lattice is found. There is one acoustic branch since the elementary cell contains one atom and displacements are one component. Assuming that the half-length of the bcc cell edge is 1, one obtains the dependence of the phonon frequency ω on the components k_i, $i = 1,2,3$, of its normalized wave vector $\mathbf{k}$:

$$\omega(\mathbf{k}) = 2\sqrt{\frac{2\gamma}{m}(1 - \cos k_1\cos k_2\cos k_3)}. \tag{13}$$

The first Brillouin zone is a 12-face polyhedron bordered by the surface resulting from the intersection of 12 planes drawn normally to the 12 directions of the type [110] at a distance of $\pi/\sqrt{2}$ from the origin of coordinates (cf., e.g., [84]). Each face is a rhombus, and all rhombuses are identical.

We are interested in the energy reflection R and transmission T coefficients of the phonons, incident on the defect planes $p_3 = 0, \pm 1$. These coefficients are defined as $R = |a_R|^2$ and $T = |a_T|^2$, where a_R and a_T are the amplitudes of the displacements $u^{p_2,p_3}_{p_1,R}$ and $u^{p_2,p_3}_{p_1,T}$ accompanying the reflected and transmitted phonons, respectively. The amplitude of the displacement associated with the incident phonon $u^{p_2,p_3}_{p_1,I}$ equals 1. It is assumed that the incident phonon propagates in the part of the lattice where the indices p_3 are negative, so the phase factors take the form $\exp[i(\varphi_g - \omega t)]$, where $\varphi_g = \sum_{j=1}^{2} k_j p_j \pm k_3 p_3$, $g = I,T,R$, the upper and lower signs correspond, respectively, to the incident (I) and transmitted (T), and to the reflected (R) phonons.

We derive $a_{R,T}$ with the aid of Eqs. (5)–(11). Intermediate calculations involve the displacements of the host atoms

$$\begin{aligned}
u^{p_2,p_3}_{p_1} &= u^{p_2,p_3}_{p_1,I} + u^{p_2,p_3}_{p_1,R}, \quad p_3 = -2,-3\\
u^{p_2,p_3}_{p_1} &= u^{p_2,p_3}_{p_1,T}, \quad p_3 = 2,3
\end{aligned}$$

displacements $u^{p_2,\pm 1}_{p_1}$ of the impurities m_2 and the displacements of impurities m_1 and m_1^*. The latter two quantities are expressed in terms of $u^{p_2,\pm 1}_{p_1}$ directly from Eqs. (9) and (10). By writing equations for combinations $u^{p_2,p_3}_{p_1} \pm u^{p_2,-p_3}_{p_1}$ and excluding $u^{p_2,1}_{p_1} \pm u^{p_2,-1}_{p_1}$, we eventually arrive at two equations for $a_T \pm a_R$. They yield the following expressions for the complex reflection a_R and transmission a_T amplitudes:

$$a_R = -\frac{e^{-i4k_3}}{2}\left[\frac{Q^{(-)}}{Q^{(-)}_*} + \frac{Q^{(+)}}{Q^{(+)}_*}\right], \tag{14}$$

$$a_T = \frac{e^{-i4k_3}}{2}\left[\frac{Q^{(-)}}{Q^{(-)}_*} - \frac{Q^{(+)}}{Q^{(+)}_*}\right], \tag{15}$$

where

$$\begin{aligned}
Q^{(\pm)} &= A + \frac{16\gamma_2^2 C^2_{k_1k_2}}{B^{(\pm)}}, \quad Q^{(\pm)}_* = A^\dagger + \frac{16\gamma_2^2 C^2_{k_1k_2}}{B^{(\pm)}},\\
A &= 0.5m\omega^2 - 4\gamma_2 - i4\gamma C_{k_1k_2}\sin k_3,\\
C_{k_1k_2} &= \cos k_1\cos k_2,
\end{aligned}$$

$$B^{(-)} = 2(\gamma_1 + \gamma_1^* + \gamma_3 + 2\gamma_2) - m_2\omega^2,$$
$$B^{(+)} = B^{(-)} - 2\gamma_3 + 16C_{k_1k_2}B,$$
$$B = \left[\frac{\gamma_1^2\cos(k_1 - k_2)}{m_1\omega^2 - 8\gamma_1} + \frac{\gamma_1^{*2}\cos(k_1 + k_2)}{m_1^*\omega^2 - 8\gamma_1^*}\right], \quad (16)$$

where $A^\dagger$ means complex conjugation of A in Eqs. (16). This operation is not applied to $B^{(\pm)}$ because in the next section phonon absorption by defect layers is studied and certain force constants entering $B^{(\pm)}$ are assumed to be complex. If all the force constants are real, then $Q_*^{(\pm)} = Q^{(\pm)\dagger}$ and, for instance, one can check that the condition of the absence of losses $T + R = 1$ holds true. The explicit expressions of R and T are omitted here.

Equations (14)–(16) allow a number of general conclusions to be made. We begin from the analysis of the behavior of $a_{T,R}$ at $k_3 \to 0$. The ratio $Q^{(-)}/Q_*^{(-)}$ tends to 1 independently of whether $k_{1,2} \equiv 0$ or they are finite. On the contrary, the limit of $Q^{(+)}/Q_*^{(+)}$ is different depending on whether $k_{1,2} \equiv 0$ or $k_{1,2}$ are finite. In the former case $Q^{(+)}/Q_*^{(+)} \to -1$ and in the latter one $Q^{(+)}/Q_*^{(+)} \to 1$. Due to Eqs. (14) and (15), $a_T \to 1$ and $a_R \to 0$ if $k_{1,2} \equiv 0$ while $a_T \to 0$ and $a_R \to -1$ if $k_1 \neq 0$ and/or $k_2 \neq 0$. These results can be interpreted as follows. In the case of vanishing $k_{1,2}$, a phonon with frequency

$$\omega = \omega_{\max}\sin(k_3/2), \quad (17)$$

where $\omega_{\max} = 4\sqrt{\gamma/m}$, is incident normally onto the defect plane, so in the limit $k_3 \to 0$ the long-wave phonons transmit freely across the defect layer. If $k_{1,2} \neq 0$, then for $k_3 \to 0$ the grazing incidence of a phonon with frequency $\omega = 2\sqrt{(2\gamma/m)(1 - \cos k_1 \cos k_2)}$ onto the defect plane occurs. Once $a_T = 0$, there is no displacement field in one part of the structure. But, since a_R tends to be equal to -1 for the grazing incidence, the incident and reflected fields add up to zero, so there is no field in the other part either [61]. The vanishing of fields on both sides of the defect means that bulk phonons cannot propagate parallel to the defect plane although the plane can have an atomic-scale thickness [61]. This feature of the reflection of the grazing-incident phonons will be analyzed with more details in Sec. V.

Thermal conductance of the defect crystal plane is determined by the phonon energy transmission coefficient T. It appears that defect monoatomic layers can dramatically modify the frequency dependence of T and even make it to vanish at certain frequencies ω_R which correspond to the *transmission antiresonances*. Indeed, from Eqs. (15) and (16) it follows that one has $a_T = 0$ provided that $B^{(+)} = B^{(-)}$. This equality results in the equation

$$\gamma_3 - \left[\frac{\gamma_1\omega_1^2 F_{k1k2}^{(-)}}{\omega^2 - \omega_1^2} + \frac{\gamma_1^*\omega_1^{*2}F_{k1k2}^{(+)}}{\omega^2 - \omega_1^{*2}}\right] = 0, \quad (18)$$

where

$$F_{k1k2}^{(\pm)} = C_{k_1k_2}\cos(k_1 \pm k_2) \quad (19)$$

and

$$\omega_1 = 2\sqrt{2\gamma_1/m_1}, \quad \omega_1^* = 2\sqrt{2\gamma_1^*/m_1^*} \quad (20)$$

are the eigenfrequencies of vibrations of defect atoms lying in the plane $p_3 = 0$.

First of all, we note that in accordance with Eq. (18), ω_R is independent of the mass m_2 of impurities in planes $p_3 = \pm 1$ and on the force constant γ_2 specifying the interaction of these impurities with host atoms. The host lattice parameters γ and m control the upper limit of the antiresonance frequency, namely, the antiresonance frequency must be smaller than the maximum $\omega_{\max}(k_{1,2})$ of the phonon frequency at the given $k_{1,2}$. As it follows from Eq. (13), the maximum frequency is reached at the boundary of the Brillouin zone.

Now, we analyze the existence of solutions of Eq. (18). No solutions exist when $\gamma_3 = 0$ and $\omega_1 = \omega_1^*$ simultaneously. If $\gamma_3 = 0$, then no direct interatomic bonds exist between impurities in the planes $p_3 = \pm 1$. If $\omega_1 = \omega_1^*$, then it can be said that plane $p_3 = 0$ is completely occupied by alike impurities (however, we note that $\omega_1 = \omega_1^*$ implies only $m_1/m_1^* = \gamma_1/\gamma_1^*$ rather than the identity of the corresponding parameters). Therefore, with $\gamma_3 = 0$ and $\omega_1 = \omega_1^*$ simultaneously, we meet the situation when only a single phonon path to cross the defect layer exists. The two-path or multipath destructive interference is impossible and, therefore, the transmission does not vanish for $\omega < \omega_{\max}$.

In the cases when $\omega_1 = \omega_1^*$ but $\gamma_3 \neq 0$ or $\gamma_3 = 0$ but $\omega_1 \neq \omega_1^*$, Eq. (18) has one solution. We discuss such particular options in Sec. IV and now we turn to the general case when $\omega_1 \neq \omega_1^*$ and $\gamma_3 \neq 0$. In this instance, there are three paths for phonon transmission across the defect, namely, two paths through different impurities in the plane $p_3 = 0$ and a third path through the next-to-nearest-neighbor interatomic bond between impurities γ_3. In general, in such 2D lattice defect the two two-path destructive-interference transmission antiresonances can occur: one antiresonance can be produced by the additional phonon path through the interatomic bond γ_3, cf. Ref. [66], and another antiresonance can be produced by the two phonon paths provided by the different defect eigenfrequencies ω_1 and ω_1^*, cf. Ref. [72].

The roots of Eq. (18) for the antiresonance frequencies $\omega_{R1,2}$ obey the biquadratic equation

$$\gamma_3\omega^4 - D_1\omega^2 + D_2 = 0, \quad (21)$$

where

$$D_1 = \omega_1^2(\gamma_3 + \gamma_1 F_{k1k2}^{(-)}) + \omega_1^{*2}(\gamma_3 + \gamma_1^* F_{k1k2}^{(+)}),$$
$$D_2 = \omega_1^2\omega_1^{*2}(\gamma_3 + \gamma_1 F_{k1k2}^{(-)} + \gamma_1^* F_{k1k2}^{(+)}), \quad (22)$$

under the condition that the roots of Eq. (21) are not equal to ω_1 and ω_1^*. By direct substitution, it can be verified that this condition is broken if either $F_{k1k2}^{(-)} = 0$ or $F_{k1k2}^{(+)} = 0$, and then one of the two roots of Eq. (21) is equal to either ω_1 or ω_1^*, respectively. Otherwise, none of the roots of Eq. (21) are equal to ω_1 or ω_1^* unless $\omega_1 = \omega_1^*$.

When $F_{k1k2}^{(\pm)} > 0$, the discriminant of Eq. (21) is positive and smaller than D_1^2, and $D_1 > 0$. Thus, the condition $F_{k1k2}^{(\pm)} > 0$ guarantees the existence of two roots ω_{R1} and ω_{R2} of Eq. (21) independently of the characteristics of defects. The transmission coefficient vanishes at these frequencies provided that they are smaller than the $\omega_{\max}(k_{1,2})$ corresponding to $k_{1,2}$.

Figure 2 shows the area of $k_{1,2}$ values where $F_{k1k2}^{(\pm)} > 0$. Outside this area, the number of the antiresonance frequencies depends on the parameters of defects. For example, let $F_{k1k2}^{(+)} < 0$.

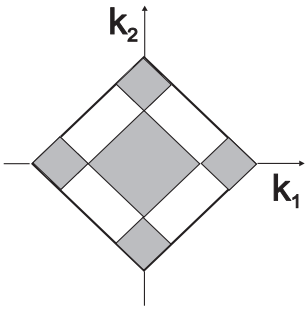

FIG. 2. Domain of $k_{1,2}$ values in plane $k_3 = 0$ where $F^{(\pm)}_{k1k2} > 0$ (gray squares). The borders of the big central square are lines $|k_1| + |k_2| = \pi/2$. Each of the four small squares is $\frac{1}{4}$ of the big square. The borders of the first Brillouin zone $|k_1| + |k_2| = \pi$ are shown by bold lines.

We choose γ_1 and γ_1^* such that $\gamma_3 = \gamma_1^*|F^{(+)}_{k1k2}| - \gamma_1 F^{(-)}_{k1k2}$, so $D_2 = 0$. Accordingly, one root of Eq. (21) is $\omega^{(1)2} = 0$. The other one $\omega^{(2)2} = \omega_1^2\gamma_1^*|F^{(+)}_{k1k2}| - \omega_1^{*2}\gamma_1 F^{(-)}_{k1k2}$ is positive or negative or equal to zero depending on the ratio between ω_1^2 and ω_1^{*2}. Therefore, we have either one or two, or no, antiresonances.

An example of the spectrum of the coefficient T is shown in Fig. 3. The symbol ω stands for the reduced frequency $\omega/\omega_{\max}$. It is seen that the reduced frequencies of the antiresonances, $\omega_{R1} \approx 0.315$ and $\omega_{R2} \approx 0.44$, given by Eq. (21), do not depend on mass m_2 (and on the force constant γ_2) because this mass and this force constant do not affect the difference between the phonon paths through the bonds γ_1 and masses m_1 and through the bonds γ_1^* and masses m_1^* (see Fig. 1). The connection of the two transmission antiresonances shown in Fig. 3 with the difference between the two phonon paths

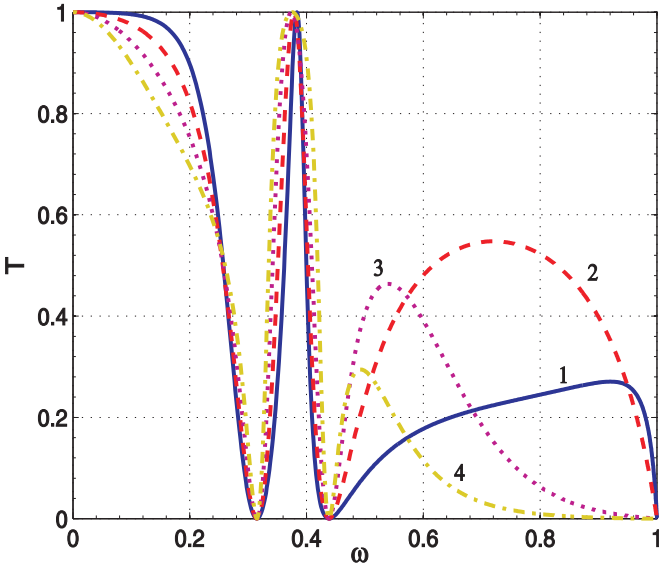

FIG. 3. Spectra of the phonon transmission coefficient T across triple defect layer versus reduced frequency at $m_2 = 0.5m$ (curve 1), $m_2 = m$ (curve 2), $m_2 = 1.5m$ (curve 3), $m_2 = 2m$ (curve 4). The other parameters are fixed and equal to $\gamma_1 = 0.25\gamma$, $\gamma_1^* = 0.5\gamma$, $\gamma_2 = \gamma$, $\gamma_3 = 2\gamma$, $m_1 = 0.75m$, $m_1^* = 3m$.

is related in turn with the phonon-interference nature of the antiresonances (see also Sec. IV below). On the other hand, the shape of the spectral lines beyond the antiresonances is significantly affected by the value of m_2, especially at frequencies higher than ω_{R2}. The change of m_2 also slightly shifts the frequency ω_T of the transmission resonance with $T = 1$, given by Eqs. (14) and (16), located in-between the frequencies of antiresonances at ω_{R1} and ω_{R2}: ω_T changes from $\omega_T \approx 0.384\omega_{\max}$ for $m_2 = 0.5m$ to $\omega_T \approx 0.375\omega_{\max}$ for $m_2 = 2m$ for the indicated in Fig. 3 parameters of the defect layer. Note that in the triple defect layer shown in Fig. 1, there can be up to two transmission resonances at the frequencies $\omega_{T1,2}$ inside the acoustic phonon band, with $0 < \omega_{T1,2} < \omega_{\max}$, in addition to the obvious transmission resonance through the 2D lattice defect at $\omega = 0$, see Figs. 6(a) and 6(b) below.

Summing up, our model predicts the existence of two transmission antiresonances provided that there are three different paths for phonons to cross the atomic-scale defect layer. The spectral positions of the antiresonances are determined by the frequencies of two different vibrational eigenmodes of the defect atoms and the difference between the paths is due to different masses and/or different interatomic bonds of the defects. The independence of the antiresonance frequencies in Fig. 3 on the mass m_2 and force constant γ_2 is explained by the independence of the characteristic frequencies ω_1 and ω_1^* on the parameters m_2 and γ_2 that do not affect the difference between the two phonon paths [see Eq. (20) and Fig. 1]. In Sec. IV below we describe the phenomenon of the phonon-interference-induced transparency of the defect crystal plane, which is caused by relatively weak splitting of the frequencies of vibrational eigenmodes of the defect atoms.

According to our model, the antiresonances occur within a fairly wide domain of the Brillouin zone embracing the direction of normal incidence. As applied to the situation where all three acoustic phonon branches are present, one can conjecture the following conclusion about the phonon transmission. If the transmission coefficient of (quasi)longitudinal phonons incident normally onto a 2D defect vanishes at frequency ω_R, then it will vanish also for oblique incidence of (quasi)longitudinal phonons at the frequencies $\omega_R(k_1,k_2)$ depending on the wave-vector tangential components k_1 and k_2. But, the cumulative (for all polarizations) transmission coefficient will not be zero since obliquely incident (quasi)longitudinal phonons can generate the transmission of (quasi)transverse phonons. On the other hand, if the defect planes are oriented symmetrically, e.g., are parallel to the plane of symmetry, then the phonon conversion disappears at normal incidence and the conversion is weak for the phonons incident under not large incidence angles. Hence, there is a domain of the wave-vector tangential components k_1 and k_2, in which the cumulative transmission will be finite but very small around the frequency $\omega = \omega_R(k_1,k_2)$.

III. ANOMALOUS PHONON ABSORPTION BY 2D DEFECT LAYER

It is well known that attenuation can significantly change the behavior of a system in the vicinity of resonance frequencies. In this section, we analyze the effect of dissipation of the defect layer oscillations on the phonon multipath reflection

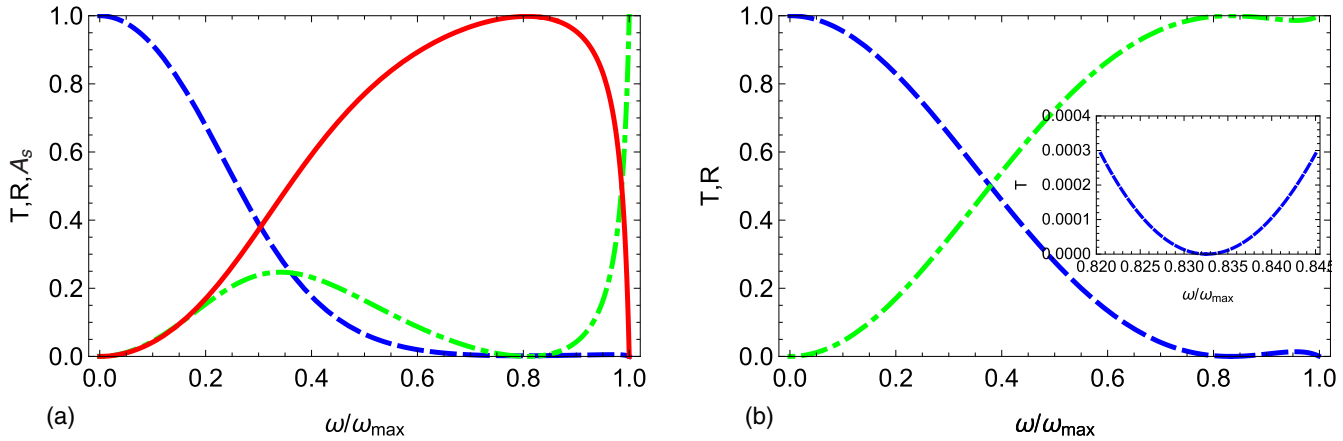

FIG. 4. (a) Spectra of phonon energy transmission T (dashed line), reflection R (dotted-dashed line), and interface absorption $A_s = 1 - T - R$ (solid line) at double-resonance defect layer in the presence of dissipation. Parameters of the defect layer are given by Eqs. (32). (b) Spectra of phonon energy transmission (dashed line) and reflection (dotted-dashed line) through double-resonance defect layer in the absence of dissipation. Parameters of the defect layer are given by Eqs. (33). Inset shows phonon transmission in the vicinity of the antiresonance.

and transmission [66]. For the sake of simplicity, the normal incidence is considered ($k_1 = k_2 = 0$) and it is assumed that $m_1 = m_1^*$ and $\gamma_1 = \gamma_1^*$. Phonon spectrum (13) reduces to Eq. (17) in this case.

Losses of the defect layer oscillations are assumed to be proportional to relative velocities of the impurity and host atoms. They can be incorporated into our model by replacing the real force constants $\gamma_{1,3}$ with the complex quantities $\gamma_{1,3} = \gamma'_{1,3} - i\gamma''_{1,3}$, with

$$\gamma''_{1,3} \propto \omega\chi_{1,3}, \tag{23}$$

where $\chi_{1,3}$ are real constants. The exact nature of phonon dissipation, e.g., due to lattice anharmonicity, is not crucial in our approach and is not discussed here.

The expressions for the transmission and reflection amplitudes (14) and (15) in the case of normal incidence ($k_1 = k_2 = 0$) and for $m_1 = m_1^*$, $\gamma_1^* = \gamma_1$, and $\gamma_2 = \gamma$, can be written explicitly in an acceptably concise form as

$$a_T = \exp(-2ik)\frac{N_t(\omega)}{\Delta(\omega)}, \tag{24}$$

$$a_R = \exp(-2ik)\frac{N_r(\omega)}{\Delta(\omega)}, \tag{25}$$

where

$$\Delta(\omega) = \{\gamma_1 + \gamma_3/2 - m_2\omega^2 + \gamma[1 - \exp(ik)]\}\big[2\gamma_1^2 + (2\gamma_1 - m_1\omega^2)\{m_2\omega^2 - \gamma_1 - \gamma[1 - \exp(ik)]\}\big], \tag{26}$$

$$N_t(\omega) = 2i\sin(k)\gamma\big[\gamma_1^2 + \gamma_3(2\gamma_1 - m_1\omega^2)/4\big], \tag{27}$$

$$N_r(\omega) = -[\Delta(\omega) + 2i\gamma\sin(k)\{\gamma_1^2 + (2\gamma_1 - m_1\omega^2) \times [m_2\omega^2 - \gamma_1 - \gamma_3/4 - \gamma(1 - \exp(ik))]\}]. \tag{28}$$

With the use of Eqs. (24)–(28), one can find the following four equations for the defect masses and the real and imaginary components of the defect force constants, which determine the conditions for the occurrence of the *anomalous interface absorption* with the total nontransmission and total nonreflection, when $T = R = 0$, and the value of the corresponding antiresonance frequency ω_R:

$$\omega_R = \sqrt{\frac{2\gamma_1' + \gamma_3'}{2m_2 - m}} = \sqrt{\frac{2\gamma_1' + 4\gamma_1'^2/\gamma_3'}{m_1}}, \tag{29}$$

$$\frac{\gamma_1''}{\gamma_3''} = \frac{\gamma_1'^2}{\gamma_3'^2}\frac{2}{1 + 4\gamma_1'/\gamma_3'}, \tag{30}$$

$$\frac{\gamma_1'' + \gamma_3''/2}{\gamma} = 2\frac{\omega_R}{\omega_{max}}\sqrt{1 - \omega_R^2/\omega_{max}^2}. \tag{31}$$

The four equations (29)–(31) originate from the nullification of the two, transmission and reflection, complex amplitudes. Equations (29)–(31) show that the anomalous interface absorption occurs under the *double-resonance* conditions and that significant difference between imaginary components of the force constants γ_1 and γ_3 in the defect layer should be present [66].

Figures 4(a) and 4(b) illustrate the relevant situation. Figure 4(a) shows the spectra of phonon energy transmission T, reflection R, and interface absorption $A_s = 1 - T - R$ by the internal crystal plane completely filled with heavy-isotope atoms, with the mass ratio 2.59 between the defect and host atoms which corresponds to the case of Ge-like atoms in a lattice of Si-like atoms. The following parameters of the defect layer, which exactly track the relations given by Eqs. (29)–(31), were used in the calculations:

$$\gamma_1(\omega) = \big[1 - i1.04(\omega/\omega_{max})\sqrt{1 - \omega^2/\omega_{max}^2}\big]\gamma,\ \gamma_2 = \gamma,$$
$$\gamma_3(\omega) = \big[0.772 - i1.92(\omega/\omega_{max})\sqrt{1 - \omega^2/\omega_{max}^2}\big]\gamma,$$
$$m_1 = 2.59m,\ m_2 = m. \tag{32}$$

Figure 4(b) shows the spectra of the double-resonance transmission and reflection with no absorption in the defect

layer. The parameters of the model are the following:

$$\gamma_1 = \gamma,\ \gamma_2 = \gamma,$$
$$\gamma_3 = 0.772\gamma,\ m_1 = 2.59m,\ m_2 = m. \tag{33}$$

It is seen in Fig. 4(a) that the total interface absorption of the incident phonon takes place and spectral width of the absorption line is very broad. The shape of the anomalous interface absorption line is very different from the asymmetric Lorentzian shape which is characteristic for the shape of the absorption line produced by the Fano resonance [83]. With the increase of the mass of heavy defect atoms filling the crystal plane, e.g, in the case of Sn-like atoms in the lattice of Si-like atoms with the mass ratio 4.23, the antiresonance frequency ω_R decreases and the spectral width of the absorption line further increases. From the comparison of Figs. 4(a) and 4(b), one can conclude that the change of spectrum of the reflection coefficient $R(\omega)$, caused by surface dissipation in the presence of two-path phonon interference, is much more substantial than that of the transmission coefficient $T(\omega)$. As one can see in Fig. 4(b), the double-resonance dissipationless transmission through the planar defect, which is accompanied by the two-path phonon interference, does not show the sequence of the transmission resonance and transmission antiresonance, which in some cases is characteristic for the single-resonance transmission with the phonon-interference effects. In the inset in Fig. 4(b), we show the phonon transmission in the vicinity of the antiresonance at the frequency $\omega_R \approx 0.832\omega_{\max}$, given by Eqs. (29), which is not followed by the transmission resonance [see also line 4 in Fig. 17(c) below].

It is worth comparing the anomalous interface phonon absorption, shown in Fig. 4(a), with the superscattering of photons in a planar photonic structure: in both cases of phonons [66,72,73] and photons [85], the interference overlap between two interface resonance eigenmodes is crucial and dissipative parameters of the two interfering eigenmodes are substantially different.

IV. PHONON SCATTERING BY CHESSBOARD-TYPE MONOLAYER AND PHONON-INDUCED TRANSPARENCY OF THE METASURFACE

The sharp transition from total reflection to total transmission and back again to total reflection is characteristic for the systems which show phonon analog of electromagnetically induced transparency. The latter is characterized by the occurrence of narrow transmission band for photons on the low-transmission background [86,87]. Below, we show that phonon analog of electromagnetically induced transparency can be realized in the crystal plane partially filled with resonance defects in the chessboard manner (see Fig. 1).

We assume in our model that $m_2 = m$, $\gamma_2 = \gamma$ and that the defect layer is merely a single crystal plane in which two types of impurities occupy positions in the chessboard order. This case will be referred to as the chessboard (CB) model. We neglect here the dissipation in the impurity layer, i.e., the γ_1 and γ_1^* force constants are assumed to be real.

The chessboard order in 2D atom distribution naturally creates two different phonon paths through the defect plane. One of them goes through the impurity bond γ_1 and the other goes through the impurity bond γ_1^* (see Fig. 1). Examination of Eq. (18) reveals that for $\gamma_3 = 0$, a single antiresonance exists at the frequency

$$\omega_R = \omega_1\omega_1^*\sqrt{\frac{\gamma_1 F_{k1k2}^{(-)} + \gamma_1^* F_{k1k2}^{(+)}}{\gamma_1\omega_1^2 F_{k1k2}^{(-)} + \gamma_1^*\omega_1^{*2} F_{k1k2}^{(+)}}}, \tag{34}$$

provided that the radicand in Eq. (34) is positive and neither $F_{k1k2}^{(-)}$ nor $F_{k1k2}^{(+)}$ is equal to zero. The latter condition stems from the fact that the antiresonance does not exist exactly at the frequencies ω_1 and ω_1^* from Eq. (20), as it follows from Eq. (18). Note that in Eq. (34), $F_{k1k2}^{(\pm)} = \cos(k_1 \pm k_2)$, since the factor C_{k1k2} entering into the definition of $F_{k1k2}^{(\pm)}$ in Eq. (19) is canceled. If $k_1 = 0$, then ω_R does not depend on k_2. The analogous situation takes place in the plane $k_2 = 0$. Note also that the case under consideration clearly shows that $a_T = 0$ cannot be attributed to any one-path interference of the Fabry-Pérot type: the key role plays the difference in the characteristics of the impurities in the plane $p_3 = 0$, namely, the condition that $\omega_1 \neq \omega_1^*$. The latter is equivalent to the atomic-scale lateral inhomogeneity of the 2D defect layer, which provides the two different phonon paths through the layer [66,72].

Nonexistence of the antiresonances under the condition $\omega = \omega_1$ or ω_1^* can be qualitatively explained as follows. According to Eqs. (9) and (10), the amplitudes u_0 and u_0^* of the impurities m_1 and m_1^*, respectively, obey the equations

$$\begin{aligned}(\omega^2 - \omega_1^2)u_0 &= 0.5\omega_1^2 C_{k1k2}(u_1^{(+)} + u_1^{(-)}),\\ (\omega^2 - \omega_1^{*2})u_0^* &= 0.5\omega_1^{*2} C_{k1k2}(u_1^{(+)} + u_1^{(-)}),\end{aligned} \tag{35}$$

where $u_1^{(+)}$ and $u_1^{(-)}$ are the amplitude of the displacements of the atoms in planes $p_3 = 1$ and -1, respectively. If $\omega = \omega_1$, then in view of Eq. (35) one has $u_1^{(+)} + u_1^{(-)} = 0$. Hence, $u_0^* = 0$ and one of the two phonon paths is blocked, so there is no interference. If $\omega_1 = \omega_1^*$, then the two impurities move likely. Thus, there is always only a single path for phonons. Therefore, the interference and the related anomalous feature (antiresonance) in the transmission through the monolayer defect are absent.

The transmission coefficient at $\omega = \omega_1$ equals

$$T = \frac{64\gamma^2 C_{k1k2}^2 \sin^2 k_3}{\left[4(\gamma_1 + \gamma_1^*) - m\omega_1^2\right]^2 + 64\gamma^2 C_{k1k2}^2 \sin^2 k_3}, \tag{36}$$

where the k_3 value corresponds to $\omega = \omega_1$. In deriving this expression, we have taken the advantage of the facts that at $\gamma_2 = \gamma$ the expression for A in Eq. (16) reduces to $A = -i4\gamma C_{k1k2}\exp(-ik_3)$ and that $B^{(+)}$ in Eq. (16) becomes infinite at $\omega = \omega_1$.

The CB model can be used for the analytical description of phonon transmission through internal crystal plane in a model bcc cubic lattice of Si-like atoms, partially filled with Ge-like defect atoms, which can serve as interference phonon metamirror with the transmission antiresonances in the vicinities of frequencies of resonance modes of Ge-like defect atoms in the terahertz frequency range and which were previously studied by molecular dynamics simulation [74–76]. The CB model

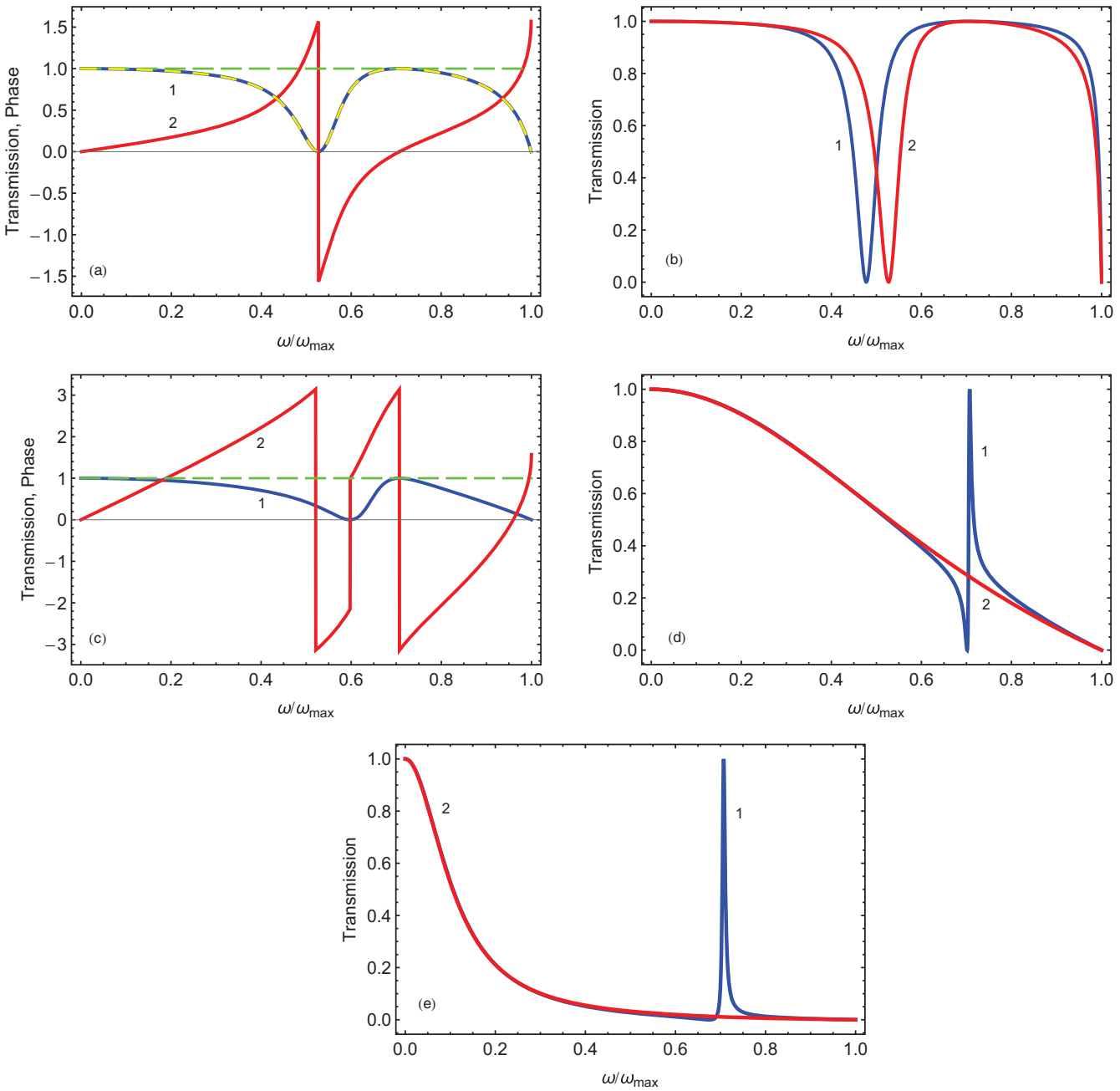

FIG. 5. (a) Spectrum of energy transmission (line 1) and phase of transmission amplitude (line 2) in the CB model with $\gamma_1 = \gamma_1^* = \gamma_2 = \gamma$, $\gamma_3 = 0$, $m_1^* = m_2 = m$, $m_1 = 2.59m$, where blue line 1 is obtained with the lattice dynamics for the model in Fig. 1, which visually coincides with the yellow line 1 given by Eq. (37) with $G = 0.2$, dashed line shows total transmission with $T = 1$. (b) Spectrum of energy transmission through the crystal plane filled with heavy-isotope atoms with $m_1 = m_1^* = 2.59m$ with filling fraction $f_d = 0.25$, obtained with the lattice dynamics for the model in Fig. 1 (line 1) and given by Eq. (37) with $G = 0.008$ (line 2). (c) Spectrum of energy transmission (line 1) and phase of transmission amplitude (line 2) through the crystal plane filled with heavy-isotope atoms with $m_1 = m_1^* = 2.59m$ and $f_d = 0.75$, dashed line shows total transmission with $T = 1$. (d), (e) Spectrum of energy transmission through the crystal plane filled with heavy-isotope atoms with $m_1 = m_1^* = 2.59m$ (d) or $m_1 = m_1^* = 10m$ (e), with $f_d = 0.99$ (lines 1) or $f_d = 1$ (lines 2).

for such system corresponds to $m_1^* = m_2 = m$, $m_1 = 2.59m$, and $\gamma_1 = \gamma_1^* = \gamma_2 = \gamma$, $\gamma_3 = 0$ in Fig. 1. In Fig. 5(a), we plot both the normal-incidence energy transmission coefficient (line 1) and the phase of the transmission amplitude (line 2) at such internal crystal plane. As one can see in this figure, the transmission antiresonance at $\omega_R/\omega_{\max} \approx 0.53$ is accompanied by the sharp change by π of the phase of the transmission amplitude, which is a characteristic feature of the destructive-interference antiresonance: the lattice waves traversing the defect plane through two different paths mutually cancel one another which results in zero phonon energy transmission. Similar sharp change by π of the phase of transmission amplitude accompanies all the considered in this paper interference antiresonances. One can also see in Fig. 5(a) that the total transmission resonance, at $\omega_T/\omega_{\max} = 1/\sqrt{2}$, is accompanied by the phase of the transmission amplitude equal

to zero, which is characteristic for the *constructive-interference* resonance [see also Fig. 5(c)].

From Eqs. (15) and (16), we get the following compact expression for the energy transmission coefficient for the CB model (see also [66,74,75]):

$$T(\omega) = \frac{\left(\omega^2 - \omega_R^2\right)^2\left(\omega_{\max}^2 - \omega^2\right)}{\left(\omega^2 - \omega_R^2\right)^2\left(\omega_{\max}^2 - \omega^2\right) + G\omega^2\left(\omega^2 - \omega_T^2\right)^2}, \quad (37)$$

where ω_R and ω_T are the frequencies of the transmission antiresonance and transmission resonance, respectively, $\omega_R < \omega_T < \omega_{\max}$. Here, G is the real positive coefficient, which gives the spectral width of the transmission dip and which for the plane waves can be related with the filling fraction f_d of the heavy-isotope Ge-like atoms in the crystal plane of the lattice of Si-like atoms. In the CB model, which corresponds to $f_d = 0.5$, the frequencies of the transmission antiresonance and transmission resonance are, respectively, $\omega_R/\omega_{\max} = 1/\sqrt{m_1/m + 1}$ and $\omega_T/\omega_{\max} = 1/\sqrt{2}$, and the coefficient $G = 0.2$. The plot for the energy transmission coefficient, given by Eq. (37) with these control parameters, yellow line 1 in Fig. 5(a), is visually indistinguishable from the blue line 1 in Fig. 5(a), obtained by numerical solution of the lattice-dynamics equations for the considered model. We note that in the case of the crystal plane in the cubic lattice of Si-like atoms filled with Ge-like atoms, the antiresonances are in the terahertz frequency range: $\omega_R \approx 6.3$ THz for longitudinal phonons (see [74–76]).

We assume that $G \propto f_d^2$, which corresponds to cooperative superradiant phonon emission of defect atoms in the internal crystal plane. In optics, the radiated intensity $\propto f_d^2$ is related with the Dicke superradiant emission [88] from a collection of identical excited atoms due to cooperative interaction between the small-size emitters and common coherent radiation (see, e.g, Ref. [89] for a review). In the case of phonon emission, the superradiance occurs due to the phonon wavelength larger than the effective thickness of the defect layer and correspondingly larger than the effective size of the identical emitters of coherent lattice waves. Using the fitting value of $G = 0.2$ for $f_d = 0.5$, we get $G \approx 0.8 f_d^2$ for the arbitrary partial filling with $f_d \leqslant 0.5$. In Fig. 5(b), we plot the transmission coefficients through the internal crystal plane in the lattice of Si-like atoms, periodically filled with heavy-isotope Ge-like atoms with $f_d = 0.25$, which corresponds to one Ge-like atoms per three Si-like atoms in the each square plaquette with 2×2 atoms in the defect crystal plane. In this plot, line 1 is obtained with the use of lattice dynamics while line 2 is given by Eq. (37) with $\omega_R/\omega_{\max} = 1/\sqrt{m_1/m + 1} = 0.53$ for $m_1 = 2.59m$, $\omega_T/\omega_{\max} = 0.71$, and $G = 0.8 f_d^2 = 0.05$. As one can see in Fig. 5(b), there is small shift of the antiresonance to lower frequency with respect to the prediction of Eq. (37), but the reduced, with respect to that in Fig. 5(a), spectral width of the antiresonance is well reproduced. For $f_d \ll 1$, the antiresonance transforms into very narrow transmission dip, with the spectral width $\Delta\omega/\omega_{\max} \propto f_d^2$ at the reduced frequency which for $f_d \to 0$ tends to $\omega_1/\omega_{\max} = \sqrt{m/(2m_1)} = 0.439$, on the background of almost total transmission for the rest of frequencies in the phonon band, for $0 \leqslant \omega < \omega_{\max}$. But, in the case of the incidence of Gaussian phonon wave packet with a finite spatial width (coherence length) l, spectral width $\Delta\omega$ of very narrow antiresonance, in the limit $f_d \ll 1$, is determined by the coherence length of the wave packet, $\Delta\omega = v_g/(2l)$, where v_g is phonon group velocity at $\omega = \omega_R$ and $\lambda = \lambda_R$, see also [74,75]. Therefore, the width of the narrow transmission antiresonance at the two-phonon-path defect crystal plane can provide a measure of the coherence length of the phonon wave packet, similar to the width of the Hong-Ou-Mandel dip in the detection probability of the output photons produced by the two-photon destructive interference (see [78–82]). It is worth noting that because of shorter λ_R, the plane-wave limit for phonon wave packets $l \gg \lambda_R$, necessary for the existence of the sharp and deep interference antiresonance, is easier to realize for the single-atom scatterers than for the defect-atom nanoparticles embedded in a matrix, that also produce phonon-interference antiresonances [90]. It is essential in this connection that one can attribute the de Broglie–type wavelength λ_R, which is determined by the position of the antiresonance frequency ω_R in the corresponding branch of phonon dispersion in the matrix and which governs the interference effects in phonon scattering by the defects, both to single defect atoms and to defect-atom nanoparticles embedded in the matrix.

On the other hand, for higher filling fraction $f_d > 0.5$, the form of the transmission line changes and can not be properly described with Eq. (37). In Fig. 5(c), we plot both the transmission coefficient (line 1) and the phase of the transmission amplitude (line 2) for the internal crystal plane in the lattice of Si-like atoms, periodically filled with heavy-isotope Ge-like atoms with $f_d = 0.75$, which corresponds to three Ge-like atoms per one Si-like atom in each square plaquette with 2×2 atoms in the defect crystal plane. As one can see in this figure, the transmission antiresonance is accompanied by the sharp change by π of the phase of the transmission amplitude, like in Fig. 5(a), while the transmission resonance at $\omega_T/\omega_{\max} \approx 0.71$ is accompanied by the 2π (equivalent to zero) phase change, also like in Fig. 5(a), which is characteristic for the constructive-interference resonance. With the increase of f_d beyond 0.5, the antiresonance frequency ω_R approaches the transmission-resonance frequency ω_T. For the crystal plane, almost fully filled with heavy-isotope defects, with $1 - f_d \ll 1$, the transmission line contains very narrow resonance peak of total transmission, at $\omega_T/\omega_{\max} \approx 1/\sqrt{2}$ and with spectral width $\Delta\omega/\omega_{\max} \propto (1 - f_d)^2$, on the background of monotonously decaying transmission line. In Fig. 5(d), we plot the transmission coefficients at the 2D defect planes with $f_d = 0.99$ of Ge-like atoms (line 1), which corresponds to 99 defect atoms per one Si-like atom in the each square plaquette with 10×10 atoms in the crystal plane, and with $f_d = 1$ (line 2), which corresponds to the crystal plane fully filled with heavy-isotope atoms. In Fig. 5(e), we plot similar spectra for the case of the model crystal plane, which is partially, with $f_d = 0.99$ (line 1), or fully, with $f_d = 1$ (line 2), filled with heavy-isotope atoms with even larger mass ratio $m_1 = m_1^* = 10m$.

Lines 1 in Figs. 5(d) and 5(e) demonstrate the constructive-interference *extraordinary phonon transmission* produced by resonance oscillations of rare host atoms, periodically distributed in the crystal plane almost fully filled with heavy-isotope defects. This phenomenon is similar to the extraordinary optical transmission through a metal film with periodic array of subwavelength holes [91]. The extraordinary optical transmission is related with the excitation of surface electromagnetic mode in the finite-thickness metal film [92]. In

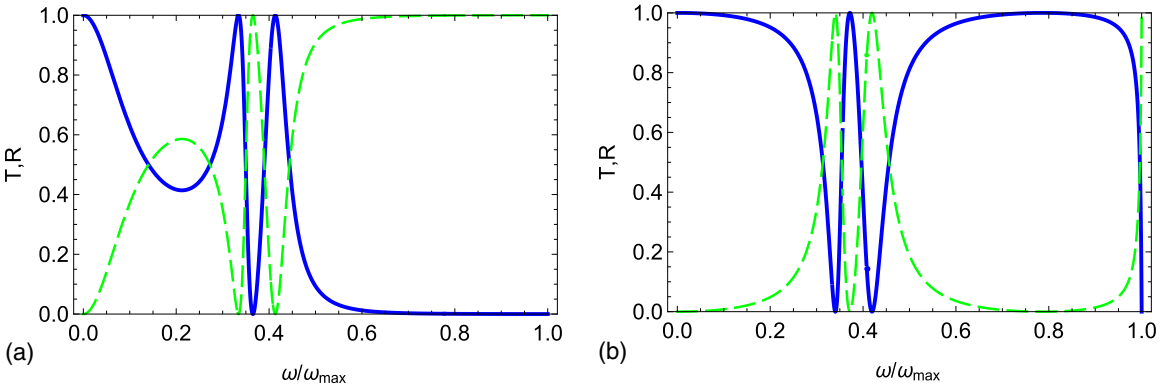

FIG. 6. Spectra of energy transmission (solid lines) and reflection (dashed lines) coefficients versus reduced frequency in the CB model with $\gamma_1 = \gamma_1^* = 0.2\gamma$, $m_1 = 0.6m$, $m_1^* = 0.9m$, and $\gamma_3 = 0$ (a) or $\gamma_3 = 4\gamma$ (b).

the case of phonons crossing crystal plane almost fully filled with heavy-isotope atoms, the close sharp transmission and reflection peaks are produced by the two-path constructive and destructive interference of the lattice waves traversing defect plane through the rare host atoms with local vibrational resonance at $\omega \approx \omega_{\max}/\sqrt{2}$ and through the surrounding them heavy isotopes.

Now, we analyze the case of relatively small splitting of the frequencies of vibrational eigenmodes of defect atoms caused by the difference in their masses and/or force constants (see Fig. 1). First, we consider the case, when the frequencies ω_1 and ω_1^* in Eq. (36) for T are approximately equal to each other. Let $\omega_1^* = \omega_1 + \Delta\omega$, where $\Delta\omega \ll \omega_1$. From Eq. (34) we get an estimate for the antiresonance frequency

$$\omega_R \approx \omega_1 + \frac{\gamma_1 F_{k1k2}^{(-)} \Delta\omega}{\gamma_1 F_{k1k2}^{(-)} + \gamma_1^* F_{k1k2}^{(+)}}. \tag{38}$$

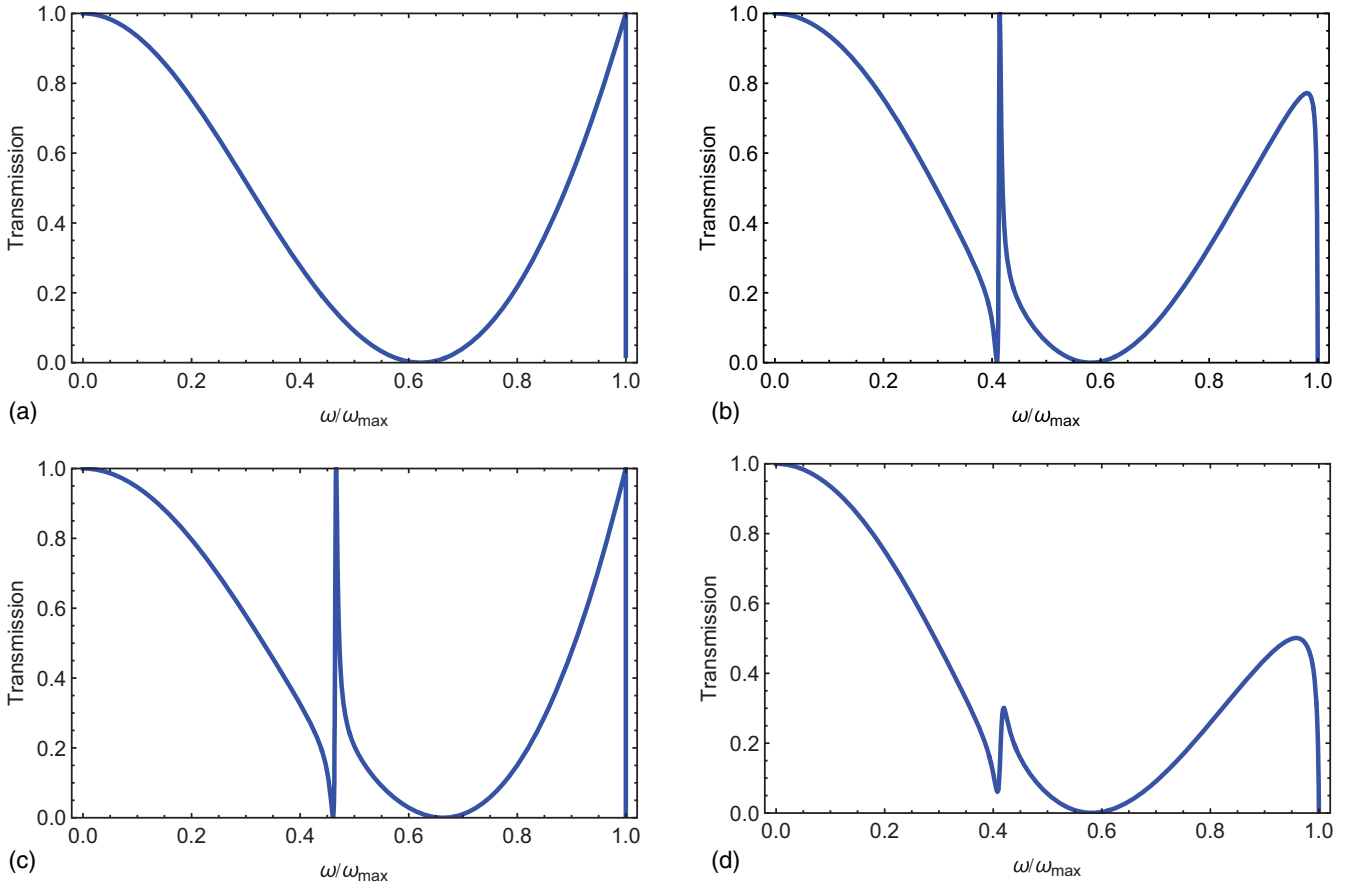

FIG. 7. Energy transmission versus reduced frequency in the CB model with (a) $\gamma_1 = \gamma_1^* = \gamma$, $\gamma_3 = 2\gamma$, $m_1 = m_1^* = 2.59m$, (b) $\gamma_1 = \gamma$, $\gamma_1^* = 0.8\gamma$, $\gamma_3 = 2\gamma$, $m_1 = m_1^* = 2.59m$, (c) $\gamma_1 = \gamma_1^* = \gamma$, $\gamma_3 = 2\gamma$, $m_1 = 2.59m$, $m_1^* = 0.8 * 2.59m$, and (d) $\gamma_1 = \gamma[1 - i0.05(\omega/\omega_{\max})]$, $\gamma_1^* = 0.8\gamma[1 - i0.05(\omega/\omega_{\max})]$, $\gamma_3 = 2\gamma[1 - i0.05(\omega/\omega_{\max})]$, $m_1 = m_1^* = 2.59m$. Spectra in panels (b)–(d) show the phonon-interference-induced transparency, which survives even in the presence of dissipation.

For $F^{(\pm)}_{k1k2} > 0$, $k_{1,2}$ fall into the gray region in Fig. 2. As a result, we meet a situation where T is around unity at two close frequencies and $T = 0$ in-between them. Figure 6(a) illustrates the frequency dependence of such type.

But, if the non-nearest-neighbor coupling γ_3 in the CB model is introduced (see Fig. 1), the transmission and reflection spectra change drastically: the additional phonon pass through the non-nearest-neighbor bonds can invert the transmission and reflection spectra in the vicinity of the resonance. In Fig. 6(b), we show the spectra of the transmission and reflection in the CB model in the *supercoupling* limit $\gamma_3 = 4\gamma$, while other parameters of the 2D defect are the same as in Fig. 6(a). In this case, the transmission antiresonance, at the frequency $\omega_R \approx 0.365\omega_{\max}$ given by Eq. (21), is replaced by the transmission resonance at the frequency $\omega_{T1} \approx 0.372\omega_{\max}$, in addition to the transmission resonance at the higher frequency $\omega_{T2} \approx 0.79\omega_{\max}$, given by Eqs. (14) and (16). This effect can be considered as the *phonon-interference-induced transparency* of 2D defect layer. The occurrence of the two antiresonances in Fig. 6(b) has the same origin as that of the two antiresonances in Fig. 3, namely, the splitting of the frequencies of two different vibrational eigenmodes of the defect atoms and the existence of three different paths for phonons to cross the atomic-scale defect layer.

The phonon-induced transparency can be even more pronounced and more similar to the electromagnetically induced transparency in the 2D defect layer with close frequencies ω_1 and ω_1^*. In Fig. 7, we show the transmission spectra through 2D defect layer with the non-nearest-neighbor supercoupling $\gamma_3 = 2\gamma$ for, respectively, (a) homogeneous layer of heavy-isotope defects with $m_1 = 2.59m$, (b) inhomogeneous layer with two different types of force constants (interatomic bonds) between defect and host atoms, with $\gamma_1 = \gamma$ and $\gamma_1^* = 0.8\gamma$, (c) inhomogeneous layer with two types of heavy-isotope defects, with $m_1 = 2.59m$ and $m_1^* = 0.8 * 2.59m$, and (d) inhomogeneous layer with two different types of complex force constants between defect and host atoms, with $\gamma_1 = \gamma[1 - i0.05(\omega/\omega_{\max})]$, $\gamma_1^* = 0.8\gamma[1 - i0.05(\omega/\omega_{\max})]$, and $\gamma_3 = 2\gamma[1 - i0.05(\omega/\omega_{\max})]$. The ratio between masses of the defect atoms in 2D layer and host atoms is equal to the mass ratio of Ge and Si atoms, in which case the force constants between different combinations of these atoms are almost identical. As one can see in Figs. 7(b) and 7(c), the phonon-induced transparency occurs at the frequency, given by Eqs. (14) and (16), $\omega_T \approx 0.41\omega_{\max}$ or $\omega_T \approx 0.47\omega_{\max}$ in 7(b) and 7(c), respectively. It is caused by the existence of two close defect eigenfrequencies in the 2D embedded layer that make nonequivalent the two phonon paths through the nearest-neighbor defect-host bonds γ_1 and γ_1^* and masses m_1 and m_1^*.

Comparison of Figs. 7(b) and 7(d) shows that the dissipation smooths out resonance features of the phonon-interference-induced transparency of the 2D defect, but does not suppress them fully. The origin of the suppression of the phonon-induced transparency is related with the incoherence of resonance oscillations at ω_1 and ω_1^*, produced by dissipation, and corresponding suppression of the constructive interference in the two phonon paths with close resonance frequencies, producing narrow transmission peak. This conclusion is confirmed by the observation that the dissipative contribution to the nearest-neighbor defect-host bonds γ_1 and γ_1^*, which form two different phonon paths, is more essential in the suppression of the phonon-induced transparency than the dissipative contribution to the non-nearest-neighbor bond γ_3, which produces the "main" antiresonance transmission dip. Indeed, the equal relatively small dissipative contributions to the bonds γ_1, γ_1^*, and γ_3 substantially suppress the constructive-interference-induced transmission peak but do not suppress the main antiresonance transmission dip at the frequency $\omega_{R2} \approx 0.58\omega_{\max}$, given by Eq. (21), which is produced by the destructive phonon interference through the additional phonon path provided by the strong bond γ_3 [see Fig. 7(d)]. It is worth noting in this connection that in the case of very close defect eigenfrequencies $\omega_1^* \approx \omega_1 \equiv \omega_D$, the width of transmission peak decreases monotonically with the decrease of the difference between the eigenfrequencies ω_1 and ω_1^*, and the frequency of the narrow phonon-induced transparency peak is determined by the defect eigenfrequency, $\omega_T \cong \omega_{R1} \approx \omega_D$, and is in general different from but is close to the frequency ω_{R2} of the relatively broad main antiresonance in the case of strong non-nearest-neighbor bond γ_3, see Eq. (21) and Figs. 7(a)–7(d).

The CB model allows also one to compare the phonon transmission across a monoatomic layer fully occupied by foreign atoms with the phonon transmission across a monoatomic layer partially filled with foreign atoms. Let $m_1^* = m$ and $\gamma_1^* = \gamma$, that is, we assume that half of the cites in the defect plane $p_3 = 0$ are occupied by the impurity atoms with mass m_1 and defect-host bond γ_1. The other half of the cites are occupied by the host atoms (we recall that the atoms with $m_2 = m$ and $\gamma_2 = \gamma$ in the CB model are the host atoms; see Fig. 1 and the beginning of this section). For the sake of simplicity, we consider the normal incidence. In this instance, like in the previous section, we use the reduced frequency $\omega/\omega_{\max} \to \omega$, which changes from 0 to 1. The symbol $\omega_{\max}$ denotes the maximum frequency of normally incident phonons [see Eq. (17)], and in the following we use the notations

$$\mu_{1,2} = \frac{m_{1,2}}{m}, \quad \tilde{\gamma}_{1,2} = \frac{\gamma_{1,2}}{\gamma}, \quad \tilde{\gamma}_3 = \frac{\gamma_3}{4\gamma}.$$

The transmission and reflection coefficients simplify to

$$T = \frac{N_T^{\mathrm{CB}}}{N_T^{\mathrm{CB}} + N_R^{\mathrm{CB}}}, \tag{39}$$

$$R = \frac{N_R^{\mathrm{CB}}}{N_T^{\mathrm{CB}} + N_R^{\mathrm{CB}}}, \tag{40}$$

where

$$\begin{aligned} N_T^{\mathrm{CB}} &= (1-\omega^2)\left(\mu_1 + \tilde{\gamma}_1^2\right)^2\left(\omega^2 - \omega_R^2\right)^2, \\ N_R^{\mathrm{CB}} &= 16\omega^2\mu_1^2(\tilde{\gamma}_1 - 1)^2\left(\omega^2 - \omega_{T1}^2\right)^2\left(\omega^2 - \omega_{T2}^2\right)^2, \end{aligned} \tag{41}$$

where the reduced antiresonance frequency ω_R, normalized by $\omega_{\max}$, is given by the expression

$$\omega_R = \sqrt{\frac{\tilde{\gamma}_1(1+\tilde{\gamma}_1)}{2\left(\mu_1 + \tilde{\gamma}_1^2\right)}}, \tag{42}$$

and $\omega_{T1,T2}$ are the roots of the equation

$$\begin{aligned} &8\mu_1\omega_T^4(\tilde{\gamma}_1 - 1) - \omega_T^2\left[\tilde{\gamma}_1^2(2+\mu_1) + 2\tilde{\gamma}_1(3\mu_1 - 2) - 5\mu_1\right] \\ &\quad + \frac{\tilde{\gamma}_1}{2}[\tilde{\gamma}_1(\mu_1 + 3) + \mu_1 - 5] = 0. \end{aligned} \tag{43}$$

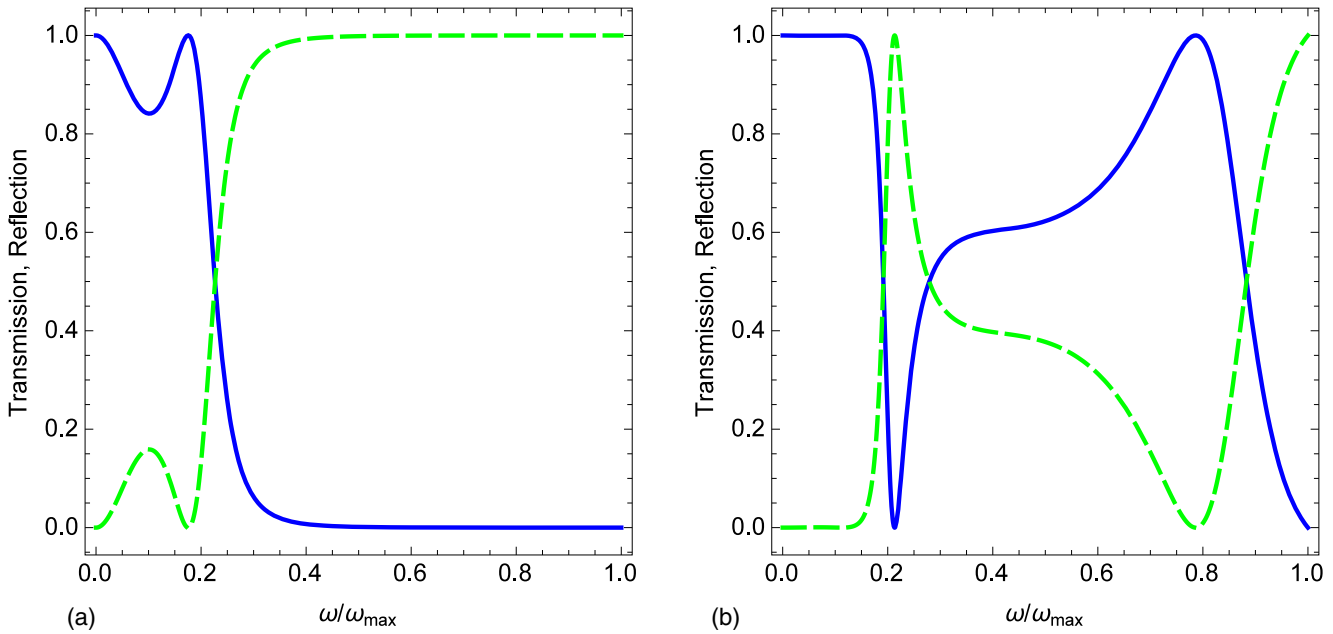

FIG. 8. Energy transmission (solid lines) and reflection (dashed lines) coefficients versus reduced frequency in the CB model with $m_1 = 2.59m$, $m_1^* = m$ and $\gamma_1 = 0.2\gamma$, $\gamma_1^* = \gamma$. Impurity filling factor is 1 in (a) and 0.5 in (b).

The transmission coefficient is zero at $\omega = \omega_R$ under the condition $\omega_R < 1$. The latter inequality restricts the values of $\tilde{\gamma}_1$ and μ_1. Similarly, the reflection coefficient R vanishes at the reduced frequencies ω_{T1} and ω_{T2} provided that they are real and smaller than 1.

Figure 8(a) depicts the spectra of T and R in the case when the plane $p_3 = 0$ is fully filled by weakly bound and heavy defect atoms. There are no transmission antiresonances, the transmission falls almost to zero at $\omega > 0.3$, and the transmission peak at the frequency $\omega_T \approx 0.18\omega_{\max}$, given by Eq. (49) below, is produced by the one-path constructive-interference Fabry-Pérot–type total transmission through the monolayer of the weakly bound impurity atoms (see also Refs. [58,61–66]). If the same impurities occupy only a half of lattice sites in the 2D layer, the antiresonance, caused by the second phonon path, occurs at the frequency $\omega_R \approx 0.21\omega_{\max}$, given by Eq. (42), at which $T = 0$ and $R = 1$ [see Fig. 8(b)]. This figure also shows that the total transmission, with $T = 1$ and $R = 0$, is realized at the frequencies $\omega_{T1} \approx 0.11\omega_{\max}$ and $\omega_{T2} \approx 0.79\omega_{\max}$, given by Eq. (43), due to the resonances with the impurity and host atoms in the crystal plane partially filled with weakly bound and heavy defect atoms. For the high filling fraction f_d of the weakly bound and heavy defect atoms, when $1 - f_d \ll 1$, the relatively broad transmission peak at $\omega_{T1} \approx 0.18\omega_{\max}$ persists together with the narrow extraordinary phonon transmission peak at $\omega_{T2} \approx \omega_{\max}/\sqrt{2}$ on the background of very low transmission at close frequencies (not shown), similar to the transmission peak shown in Fig. 5(e).

V. PHONON SCATTERING BY HOMOGENEOUS EMBEDDED MONOLAYER

Now, we consider one more option of the general model described in Sec. II (see Fig. 1). We assume that $\gamma_1 = \gamma_1^*$, $\gamma_2 = \gamma$, $m_1 = m_1^*$, and $m_2 = m$. This defect structure, which we call the FF model, implies that the plane $p_3 = 0$ is *fully filled* with the impurities of one sort. All sites not belonging to the $p_3 = 0$ plane are occupied by host atoms. The next-to-nearest-neighbor bond with the nonzero strength γ_3 couples host atoms in the plane $p_3 = -1$ with host atoms in the plane $p_3 = 1$.

Once $\gamma_1 = \gamma_1^*$ and $m_1 = m_1^*$, the frequencies ω_1 and ω_1^* in Eq. (20) are identical. In this instance, one solution of Eq. (18) for antiresonance frequency exists:

$$\omega_R = \omega_1\sqrt{1 + \frac{2\gamma_1 \cos^2 k_1 \cos^2 k_2}{\gamma_3}}. \tag{44}$$

In what follows, we confine ourselves to the scattering of normally incident phonon. The reflection and transmission coefficients read explicitly as

$$T = \frac{N_T^{\mathrm{FF}}}{N_T^{\mathrm{FF}} + N_R^{\mathrm{FF}}}, \tag{45}$$

$$R = \frac{N_R^{\mathrm{FF}}}{N_T^{\mathrm{FF}} + N_R^{\mathrm{FF}}}, \tag{46}$$

where, with the notations in Eq. (16), one has

$$N_T^{\mathrm{FF}} = \tilde{\gamma}_3^2(1 - \omega^2)\left(\omega^2 - \omega_R^2\right)^2, \tag{47}$$

$$N_R^{\mathrm{FF}} = (1 - \tilde{\gamma}_1 - \tilde{\gamma}_3)^2\omega^2\left(\omega^2 - \omega_T^2\right)^2. \tag{48}$$

Here, the symbol ω stands for the reduced frequency $\omega/\omega_{\max}$,

$$\omega_T = \sqrt{\frac{\tilde{\gamma}_1}{4\mu_1}\frac{2 - (1 + \mu_1)(2\tilde{\gamma}_3 + \tilde{\gamma}_1)}{1 - \tilde{\gamma}_1 - \tilde{\gamma}_3}}, \tag{49}$$

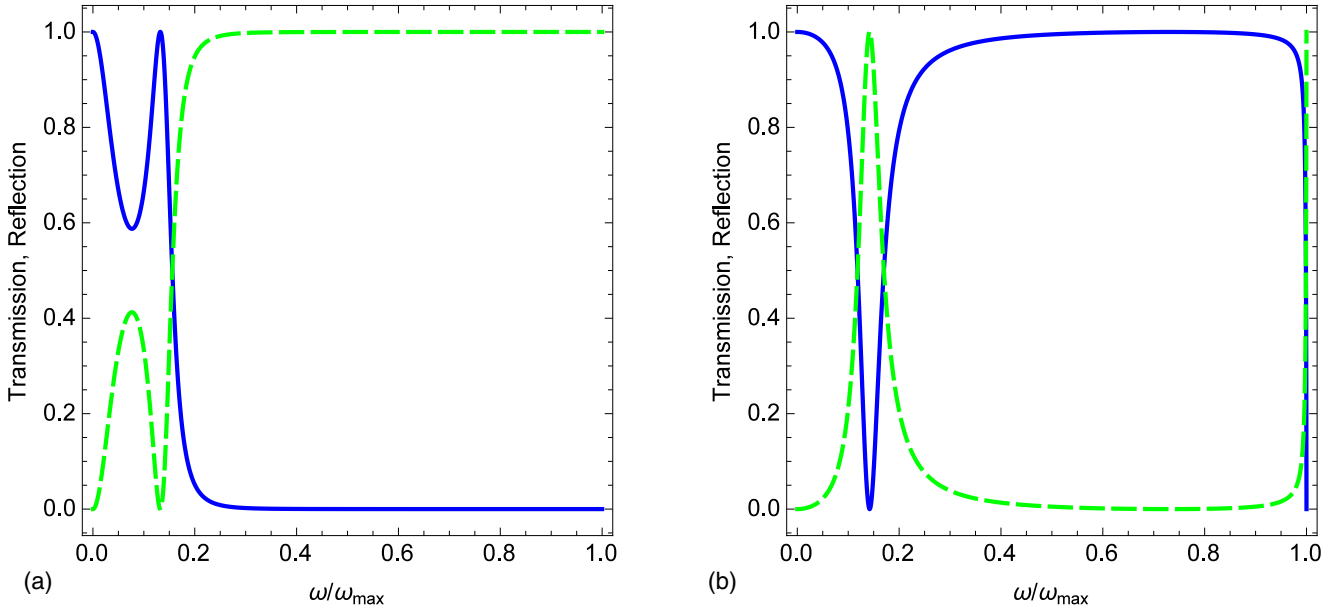

FIG. 9. Coefficients of phonon energy transmission (solid lines) and reflection (dashed lines) versus reduced frequency through the planar defect in the FF model with $m_1 = 2.59m$, $\gamma_1 = 0.1\gamma$, and with $\gamma_3 = 0$ in (a) and $\gamma_3 = 4\gamma$ in (b).

and ω_R from Eq. (44) at $k_{1,2} = 0$, after division by $\omega_{\max}$, reduces to

$$\omega_R = \sqrt{\frac{\tilde{\gamma}_1(\tilde{\gamma}_1 + 2\tilde{\gamma}_3)}{4\mu_1\tilde{\gamma}_3}}. \tag{50}$$

The value of ω_R (50) should fulfill the inequality $\omega_R < 1$ for the transmission coefficient to vanish. This inequality restricts the minimum possible value of $\tilde{\gamma}_{3c}$, which is necessary for the appearance of the antiresonance:

$$\tilde{\gamma}_{3c} = \frac{\tilde{\gamma}_1^2}{2(2\mu_1 - \tilde{\gamma}_1)}. \tag{51}$$

With further increase of $\tilde{\gamma}_3$, $\tilde{\gamma}_3 > \tilde{\gamma}_{3c}$, the reduced antiresonance frequency ω_R decreases from 1 until $\omega_1/\omega_{\max}$. Thus, when the defect monolayer is homogeneous, i.e., fully filled with the impurity atoms of the same sort, the total reflection occurs provided that the interactions responsible for the existence of the second channel of phonon transmission, provided by the bond γ_3, are strong enough. In view of Eq. (44), this conclusion also applies to the oblique phonon incidence. In contrast to that, as it follows from Eq. (21) and as it was mentioned in Sec. IV in connection with Fig. 7, no finite lower bound exists for the (nonzero) difference between eigenfrequencies of the impurities for the occurrence of the antiresonance in the defect monolayer filled by different atoms, even in the absence of the next-to-nearest-neighbor bond γ_3, for $\gamma_3 = 0$.

Figures 9(a) and 9(b) demonstrate how the transmission and reflection can vary with the γ_3 values in the case of crystal plane fully filled with weakly bound, $\gamma_1 = 0.1\gamma$, and heavy, $m_1 = 2.59m$, defect atoms, without and with the non-nearest-neighbor bond γ_3 across the defect plane. We see in Fig. 9(a) that the transmission is high below and around the reduced frequency $\omega_T \approx 0.13$, given by Eq. (49), at which it reaches unity, and quickly decreases to zero at higher frequencies in the case of $\gamma_3 = 0$. When $\tilde{\gamma}_3$ is nonzero and becomes much larger than the critical one $\tilde{\gamma}_{3c}$ (51), the spectra of the transmission and reflection coefficients change drastically, see Fig. 9(b) and compare it with the Fig. 7(a), which shows the case of strong defect-host bonds, with $\gamma_1 = \gamma$. For the weak defect-host bonds, the transmission is close to unity for all frequencies with the exception of relatively narrow range around the antiresonance frequency $\omega_R \approx 0.14\omega_{\max}$, given by Eq. (50), which is very close to the frequency of the total transmission in the case of $\gamma_3 = 0$. In other words, there is an effective "inversion" of the total transmission and total reflection in the limits of $\tilde{\gamma}_3 \ll \tilde{\gamma}_{3c}$ and $\tilde{\gamma}_3 > \tilde{\gamma}_{3c}$ [cf. Figs. 9(a) and 9(b)]. This observation clearly demonstrates that the *additional phonon path* through the interatomic bond γ_3 can drastically change phonon transmittance of the system with almost no change in the eigenfrequency (and polarization) of the local vibrational mode resonating with the continuum of phonon eigenstates in the system, in contrast to the concept of Fano resonance.

The phenomena of total transmission and total reflection of long acoustic wave by a homogeneous ultrathin defect layer or monolayer can also be observed in the domain of angles of incidence, instead of previously considered frequency domain. To describe quantitatively these phononic effects, we will use dynamic boundary conditions for the local elastic stresses $\sigma_{ik}^{(1,2)}$ and displacements $u_i^{(1,2)}$ in the vicinity of the embedded 2D defect (see, e.g., [66,93]). For long waves and low frequencies, with $\omega \ll \omega_R$, the simplest translationally and rotationally invariant dynamic boundary conditions have the following form:

$$u_i^{(1)} = u_i^{(2)} \equiv u_i^s, \tag{52}$$

$$\sigma_{ni}^{(1)} - \sigma_{ni}^{(2)} = g_{\alpha\beta}\nabla_\alpha\nabla_\beta u_i^s + \delta_{i\beta}h_{\alpha\beta\gamma\delta}\nabla_\alpha u_{\gamma\delta}^s - D_s\triangle_\alpha^2 u_i^s - \rho_s\partial^2 u_i^s/\partial t^2, \tag{53}$$

where $\sigma_{ni} = \sigma_{ik} n_k$, n_k is a unit vector of the normal to the interface directed from the medium 1 into medium 2, $g_{\alpha\beta}$ is a symmetric two-dimensional tensor of the residual surface stresses (surface stress tensor), $h_{\alpha\beta\gamma\delta}$ is the tensor of the lateral elastic moduli of the two-dimensional defect layer, D_s is (isotropic) bending stiffness of the 2D defect layer, $u^s_{\alpha\beta}$ is a symmetric tensor of two-dimensional deformations, ρ_s is an excess mass of the embedded layer per unit surface (interface) area. Here, the Latin indices take the values 1,2,3 while the Greek indices take the values 1,2 and label the coordinate axes in the (x, y) plane of the interface. In Ref. [66], more complicated boundary conditions were proposed, which take into account the displacement of the 2D defect layer as an independent dynamical variable and can also be used for the macroscopic description of 2D defects, but we will not discuss them here.

The following five phononic effects can be observed with the use of Eqs. (52) and (53).

(1) Change from the total transmission to total reflection of grazing-incident long-wave acoustic waves, which is caused by the change of the dynamic parameters of the 2D embedded monolayer [61,62].

(2) Total transmission, $T = 1$, $R = 0$, of transverse acoustic waves at the "critical angle" of excitation of bulk longitudinal wave $\Theta_l = \arcsin(v_t/v_l)$, where $v_{t,l}$ are velocities of transverse and longitudinal acoustic waves [69].

(3) Total reflection, $T = 0$, $R = 1$, of transverse acoustic waves for the incidence angle $\Theta_R > \Theta_l$, that corresponds to the excitation of the pseudosurface quasilongitudinal wave, whose velocity is smaller than the speed of bulk longitudinal wave in the direction parallel to the defect plane [67–71].

(4) Anomalous surface absorption, $A_s = 1 - T - R$, of the incident transverse acoustic wave by 2D defect monolayer in the solid with low attenuation of sound waves, when one half of the incident energy of the long acoustic wave is absorbed by the monolayer, $A_s = 0.5$, $T = R = 0.25$ [69,70].

(5) Softening of the flexural surface acoustic wave, localized at the defect plane, caused by negative (compressive) surface stress g_{xx} and finite bending stiffness D_s of the 2D elastic layer. Softening of the flexural surface acoustic wave results in periodic static bending deformation (modulation) of the interface layer with the definite wave number k_{x0}. The softening of the flexural surface acoustic wave in a sandwichlike elastic structure presents a dynamical counterpart of purely static phenomenon of the buckling of the plate sandwiched in the compressively strained matrix (see, e.g., [94]). The possibility of the softening of surface acoustic Rayleigh and interface waves, triggered by negative surface stress, was noted in [61,63,95].

The phenomenon of the total reflection of the grazing-incident *long acoustic waves* by an *embedded monolayer* is related with the impossibility of propagation of homogeneous bulk wave along the embedded monolayer when the local velocity of acoustic phonon with corresponding polarization in the layer is different from the bulk velocity in the same direction [61,63]. But, when the local velocity of acoustic phonon in the embedded monolayer coincides with the bulk one in the same direction, the grazing-incident phonons do not suffer total reflection and experience total transmission. The total reflection at the intermediate incidence angle $\pi/2 > \Theta_R > \Theta_l$ [67–70] we relate with the two-path interference transmission antiresonance. Now, one phonon path is provided by the transverse bulk wave traversing the 2D layer, the other phonon path is provided by the pseudosurface (leaky) quasilongitudinal wave supported by the layer, and the necessary π phase difference between the paths is provided by the *incidence-angle resonance* at the excitation of the pseudosurface quasilongitudinal wave. The anomalous surface absorption occurs at the same incidence-angle resonance at the 2D defect layer in the presence of definite bulk or interface dissipative parameters. Possible softening of the surface acoustic wave at the 2D lattice defect with negative surface stress was qualitatively described in Refs. [61,63] for pure shear waves polarized in the defect plane, and here we describe similar effect for the flexural waves within the unified approach. Below, we analyze in details all the above phononic effects.

First, we introduce the four length parameters a, b, c, and d, which describe the following three surface parameters of the defect: $\rho_s = a\rho$, $g_{xx} = b\mu$, $h_{xxxx} = c\mu$, $D_s = d^3\mu$, where ρ and μ are bulk density and shear elastic modulus of the solid, which we will assume to be isotropic below in this section. All the parameters a, b, c, and d have in general the order of interatomic distance in the solid. Then, all the acoustic parameters of the solid can be made dimensionless after corresponding normalization, and the frequency of the incident phonon can be measured in v_t/a. In these dimensionless units, the transmissivity and reflectivity of the 2D defect layer are the functions of only the ratio of longitudinal and transverse bulk acoustic velocities $V_{\rm rel} = v_l/v_t$ of the isotropic solid, angle of incidence Θ, dimensionless frequency $\omega a/v_t$, and three relative defect lengths b/a, c/a, and d/a. In Fig. 10, we plot the energy transmission coefficient T of transverse phonons through the 2D defect layer, described with the use of Eqs. (52) and (53) in the case of $v_l/v_t = 2$, $c = 0.1a$, $d = 0$, and $b = 0.9a$ in the upper panel, or $b = a$ in the lower panel. According to Eq. (53), velocity of the transverse wave with vertical polarization in the 2D defect layer with $D_s = 0$, propagating along the x direction, is given by $\sqrt{g_{xx}/\rho_s} = v_t\sqrt{b/a}$. It is different from the bulk transverse velocity v_t for $b \neq a$ and coincides with it for $b = a$. In result, the transverse acoustic waves, which are incident at the angles close to $\pi/2$, are totally reflected from the 2D defect layer with $b \neq a$ (upper panel in Fig. 10) and are totally transmitted through the defect layer with $b = a$ (lower panel in Fig. 10). Figure 10 also demonstrates the total transmission at the "critical angle" of the excitation of bulk longitudinal wave $\Theta_l = \arcsin(v_t/v_l) \approx 0.52$ in both cases, and the total reflection at the incidence angle slightly larger than $\Theta_l = \arcsin(v_t/v_l) \approx 0.523$. In Fig. 11, we show the transmission through 2D defect layer versus incidence angle for transverse phonon with $\omega = v_t/a$ and $b = a$ (red line 1) or $b = 0.9a$ (blue line 2). As one can see in Figs. 10 and 11, the small change of the parameters of the 2D monolayer, from $b = a$ to $b = 0.9a$, almost does not affect the transmissivity of the 2D monolayer for nongrazing incidence but drastically suppress the transmissivity for the grazing-incident waves [61,63].

Dispersion equation for the pseudosurface wave with quasilongitudinal polarization, which is supported by the 2D defect layer described by Eqs. (52) and (53), relates the real part of

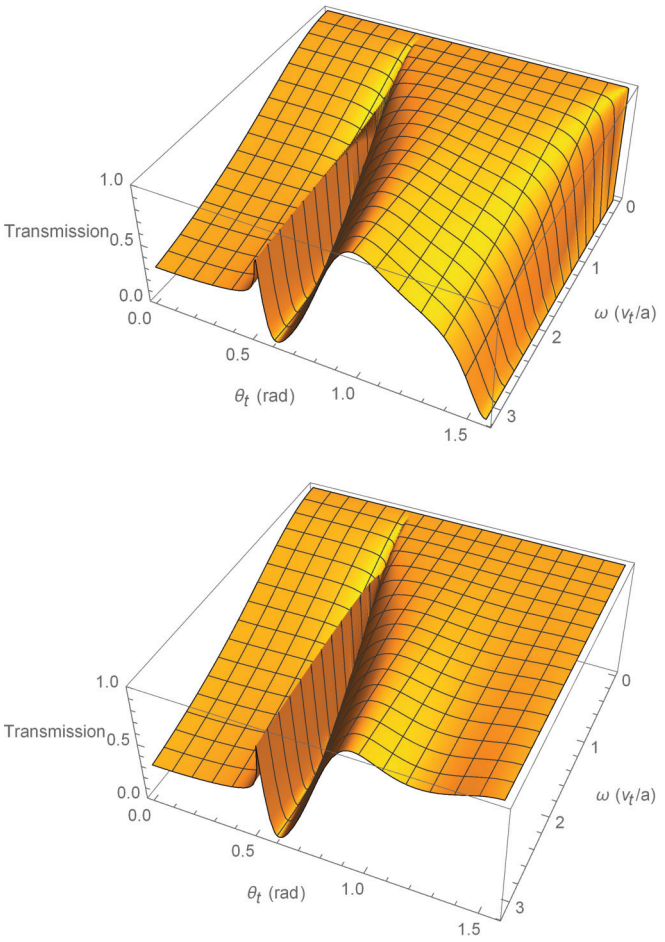

FIG. 10. Energy transmission of transverse acoustic phonons through 2D defect layer as a function of frequency and incidence angle for $v_l/v_t = 2$, $c = 0.1a$, $d = 0$ with $b = 0.9a$ (upper panel) or $b = a$ (lower panel).

its frequency with the parallel to the defect-plane component of the wave vector k_x and can be written in the following form (see Ref. [96]):

$$(q_1 + q_2)q_1q_2C_{11}C_{66} = \tfrac{1}{2}\left[\rho_s\omega^2 - (h_{xxxx} + g_{xx})k_x^2 - D_sk_x^4\right] \times \left(C_{66}k_x^2 + C_{11}q_1q_2 - \rho\omega^2\right), \quad (54)$$

where in the isotropic solid one has $q_1 = \sqrt{k_x^2 - \omega^2/v_l^2}$, $q_2 = \sqrt{k_x^2 - \omega^2/v_t^2}$, $v_l = \sqrt{C_{11}/\rho}$, $v_t = \sqrt{C_{66}/\rho}$, $C_{11} = \lambda + 2\mu$, and $C_{66} = \mu$ are the elastic moduli, with λ and μ being the Lamé coefficients.

In Fig. 12, we plot the transverse-phonon energy transmission coefficient, the phase of the transmission amplitude, and the frequency of pseudosurface quasilongitudinal wave as functions of incidence angle of the transverse phonon $\Theta = \arcsin(k_x v_t/\omega)$. Figure 12(a) shows that the excitation of the pseudosurface quasilongitudinal wave with the dispersion equation (54) is indeed related with the antiresonance, which is accompanied by the sharp change, by π, of the phase of the transmission amplitude. This sharp π change of the transmission amplitude phase is responsible for the two-path destructive-interference transmission antiresonance at this incidence angle. This plot also shows the zero, equivalent to 2π, phase change at the total-transmission incidence angle $\Theta_l = \arcsin(v_t/v_l) = \arcsin(1/2) \approx 0.5236$, which is characteristic for the constructive-interference transmission resonance [see also Figs. 5(a) and 5(c)].

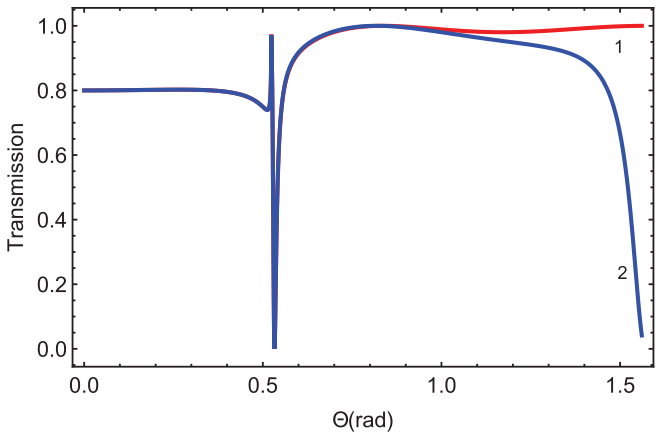

FIG. 11. Transmission of transverse acoustic phonon through 2D defect layer as a function of incidence angle for $\omega = v_t/a$, $v_l/v_t = 2$, $c = 1.1a$, $d = 0$, and $b = a$ (line 1) or $b = 0.9a$ (line 2).

In order to describe the anomalous surface absorption by the 2D defect layer, we assume that the transverse acoustic velocity in the solid v_t and the incidence angle of the transverse phonon Θ, as well as the length parameters a and b, are real quantities, while the longitudinal acoustic velocity v_l and surface elastic modulus h_{xxxx} can be the complex parameters, $v_l = v_l' - iv_l''$ and $h_{xxxx} = (c' - ic'')\mu$, whose imaginary parts take phenomenologically into account the wave attenuation due to dissipation in the bulk of the solid and in the surface of the 2D defect, respectively. Then, we write the ratios of the bulk acoustic velocities and defect length parameters c/a as $V_{\rm rel} = v_l'/v_t - i\delta_B$ and $c/a = c'/a - i\delta_S$, where $\delta_B > 0$ and $\delta_S > 0$ are the introduced dimensionless acoustic dissipative parameters. For certain values of these parameters, the anomalous surface absorption in the resonance of excitation of the pseudosurface quasilongitudinal wave can be realized, when surface absorption $A_s = 1 - T - R$ reaches the maximal value of 0.5, with $T = R = 0.25$ [69,70]. The equation, which determines the relation between the parameters δ_B and δ_S in the resonance anomalous surface absorption, has the following form (see Ref. [69]):

$$\delta_B + \delta_S\frac{(\omega a)^2}{4v_lv_t}[1 - \sin^2\Theta_R(b + c')/a]\sin^2\Theta_R = \frac{3F}{8}\left(\frac{\omega a}{v_t}\right)^3 \times [1 - \sin^2\Theta_R(b + c')/a]^3\tan\Theta_R\sin^2\Theta_R, \quad (55)$$

where Θ_R is incidence angle of transverse phonon at the resonance with pseudosurface quasilongitudinal wave, factor F has the order of unity.

In Figs. 13 and 14 we show the incidence-angle dependencies of anomalous surface absorption, frequency of pseudosurface quasilongitudinal wave with dispersion equation (54), and energy transmission and reflection coefficients at the 2D defect layer in a solid with losses of bulk longitudinal acoustic wave, with $\delta_B > 0$ and $\delta_S = 0$ in Fig. 13, and in a lossless solid

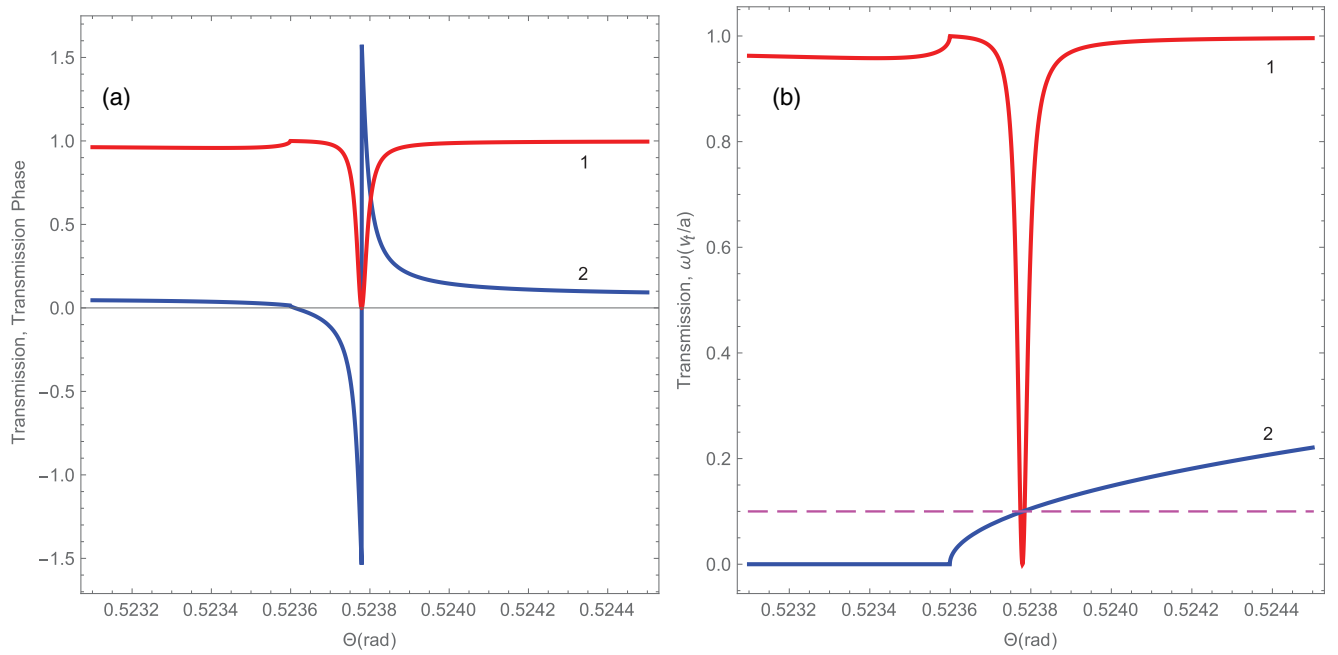

FIG. 12. (a) Transverse phonon energy transmission (line 1) and phase of transmission amplitude (line 2), (b) transmission (line 1) and frequency of pseudosurface quasilongitudinal wave (line 2), with dashed line indicating $\omega a/v_t = 0.1$, as functions of incidence angle at the 2D defect layer in the lossless solid for $\omega a/v_t = 0.1$, $v_l/v_t = 2$, $b = c = d = 0$.

with dissipative 2D defect, with $\delta_B = 0$ and $\delta_S > 0$ in Fig. 14. These figures show that the anomalous surface absorption can be realized both due to only bulk acoustic losses, when $\delta_S = 0$, and due to only surface losses in the 2D defect later, when $\delta_B = 0$.

Figures 12–14 clearly show that the transmission antiresonance [67] and anomalous surface absorption [69,70] occur at the same incidence angle, which corresponds to the excitation of the pseudosurface quasilongitudinal wave with the dispersion equation given by Eq. (54).

The value of the dimensionless bulk dissipative parameter δ_B, which realizes the maximal surface absorption for $\delta_S = 0$, scales with frequency and the length parameter a as $\delta_B \propto (\omega a/v_t)^3$ [see Eq. (55)]. This means that the anomalous surface absorption can be observed in the crystal with very low bulk acoustic losses (like, e.g., quartz crystal) with the embedded

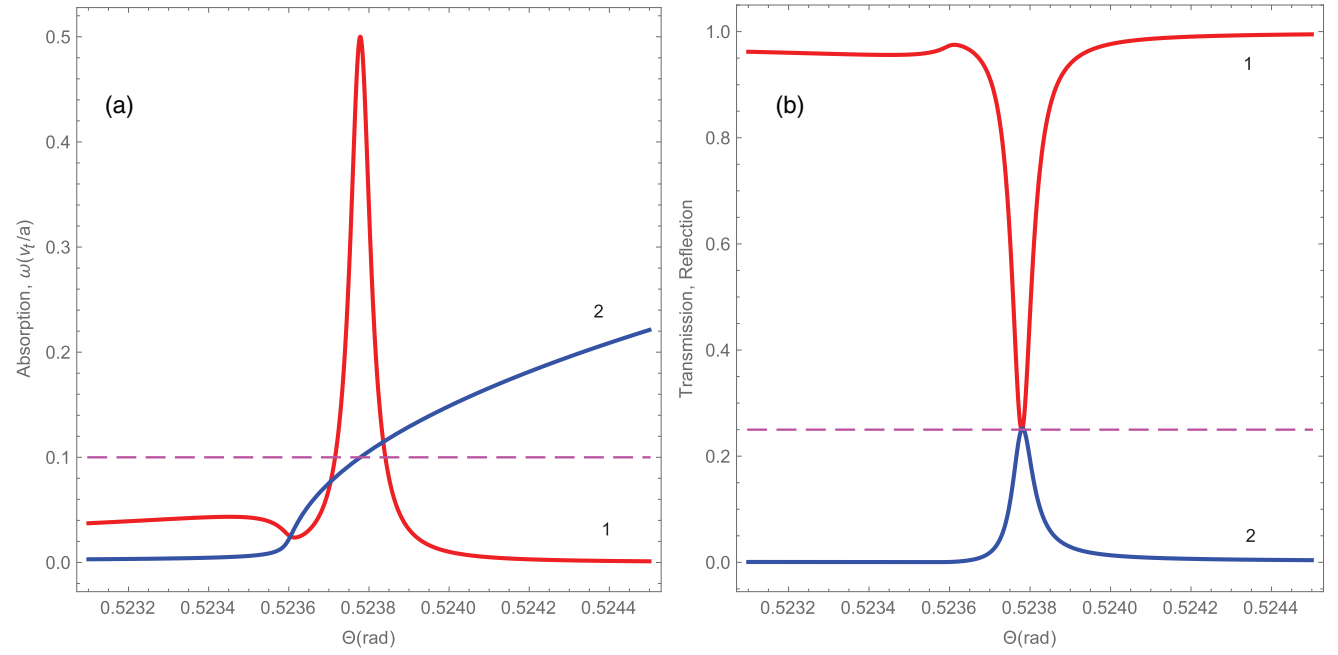

FIG. 13. (a) Anomalous surface absorption (line 1) and frequency of pseudosurface quasilongitudinal wave (line 2), with dashed line indicating $\omega a/v_t = 0.1$, (b) transverse phonon energy transmission (line 1) and reflection (line 2), with dashed line indicating the value of 0.25, as functions of incidence angle at the 2D defect layer in dissipative solid for $\omega a/v_t = 0.1$, $v_l'/v_t = 2 - i0.000055$, $b = c = d = 0$.

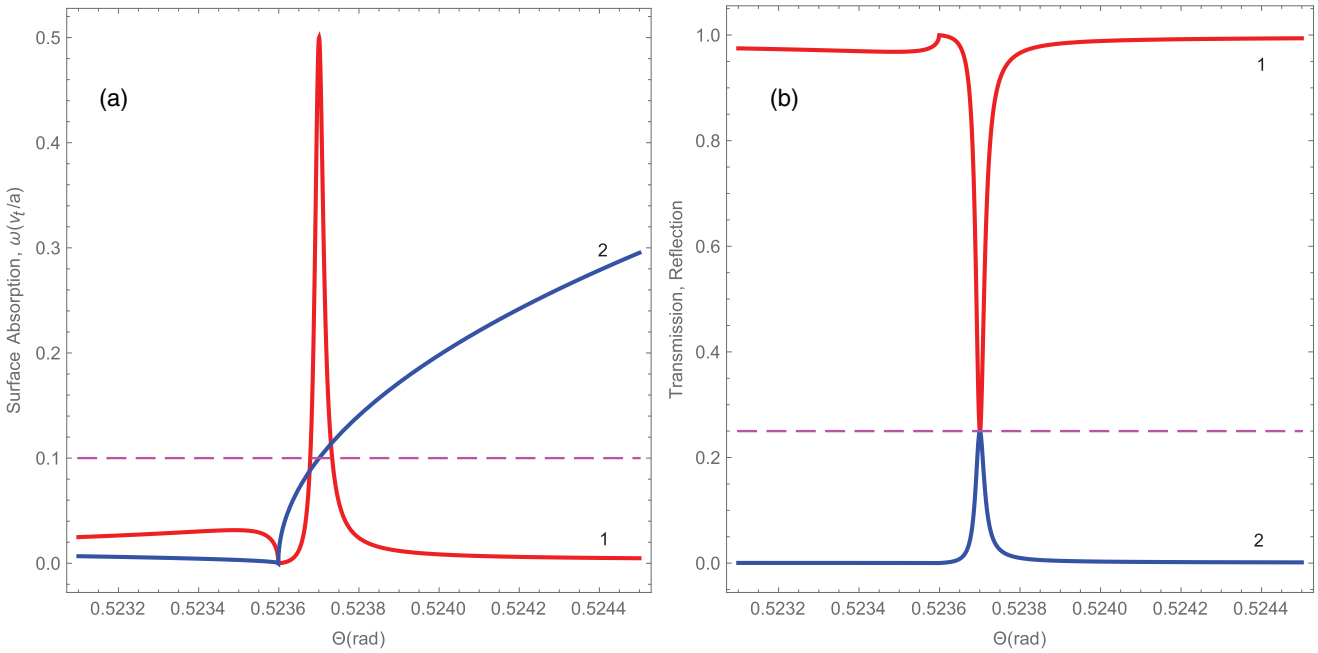

FIG. 14. (a) Anomalous surface absorption (line 1) and frequency of pseudosurface quasilongitudinal wave (line 2), with dashed line indicating $\omega a/v_t = 0.1$, (b) transverse phonon energy transmission (line 1) and reflection (line 2), with dashed line indicating the value of 0.25, as functions of incidence angle at the 2D absorbing defect layer in lossless in bulk solid for $\omega a/v_t = 0.1$, $v_l/v_t = 2$, $b = 0.9a$, $c/a = 0.1 - i0.097$, $d = 0$.

monolayer of heavy impurities, which can realize high value of the defect length parameter a. On the other hand, the phenomena of almost total resonance reflection and anomalous surface absorption in a 2D defect layer are absent in solids with the bulk losses, which greatly exceed the values given by Eq. (55) but still remain relatively weak, when $1 \gg \delta_B \gg (\omega a/v_t)^3$. In such solids, both the reflectivity R and surface absorption $A_s = 1 - T - R$ in the 2D defect layer are small while the transmissivity is high, $T \approx 1$.

To describe the softening of the flexural surface acoustic wave at the defect plane, triggered by negative (compressive) surface stress, we start with the dispersion equation for the surface wave with the quasitransverse polarization, normal to the defect plane, which is similar to the dispersion equation for the pseudosurface wave with quasilongitudinal polarization, given by Eqs. (54) with the same notations (see Ref. [96]):

$$(q_1 + q_2)q_2 C_{11}C_{66} = \tfrac{1}{2}\left(\rho_s\omega^2 - g_{xx}k_x^2 - D_s k_x^4\right) \times (C_{66}q_2 + C_{11}q_1). \tag{56}$$

The value of the negative surface stress $g_{xx} = -\,|\,g_{xx}\,|$ and the wave number k_{x0} at which the softening occurs can be found from the following two conditions (cf. Refs. [61,63,95]):

$$\omega(k_{x0}) = 0, \quad \frac{\partial\omega(k_{x0})}{\partial k_x} = 0. \tag{57}$$

In the assumption of isotropy of the elastic matrix, the required parameters are determined from Eqs. (56) and (57) and are given by the bulk modulus μ, bending stiffness D_s of the 2D elastic interface layer, and the ratio of longitudinal and transverse elastic waves in the matrix $V_{\rm rel} = v_l/v_t$:

$$\lambda_0 = \frac{2\pi}{k_{x0}} = 2\pi\left(\frac{D_s}{\mu}\right)^{1/3}\left(\frac{V_{\rm rel}^2+1}{2V_{\rm rel}^2}\right)^{1/3}, \tag{58}$$

$$|g_{xx}| = 3\left(\frac{2V_{\rm rel}^2}{V_{\rm rel}^2+1}\right)^{2/3} D_s^{1/3}\mu^{2/3}. \tag{59}$$

Since $|g_{xx}| = E_s|\epsilon_{xx}|$, where $E_s = h_{xxxx}$ is Young modulus of the 2D elastic layer and ϵ_{xx} is the in-plane strain of the matrix, from Eq. (59) we get

$$|\epsilon_{xx}| = 3\left(\frac{2V_{\rm rel}^2}{V_{\rm rel}^2+1}\right)^{2/3} \frac{D_s^{1/3}}{E_s}\mu^{2/3}. \tag{60}$$

Using Eqs. (58) and (60), we can estimate the wavelength of periodic bending λ_0 and the in-plane contraction strain in the matrix $\epsilon_{xx} = -|\epsilon_{xx}|$ for the graphene monolayer embedded in three-dimensional strained soft matrix of low-density polyethylene. For the low-density polyethylene, we take $\mu = 0.2$ GPa, $v_t = \sqrt{\mu/\rho} = 0.466$ km/s, $v_l = 2.400$ km/s, and $V_{\rm rel} = 2400/466 = 5.15$ [97], which is consistent with the molecular dynamics simulations within the coarse-grained model of amorphous polyethylene [98]. For the monolayer graphene, we take bending stiffness $D_s = 1.1$ eV and Young modulus $E_s = \rho_s v_l^2 \approx 22$ eV/Å^2, where $v_l = 21.6$ km/s is longitudinal sound velocity and $\rho_s = 7.6 \times 10^{-7}$ kg/m^2 is mass density per unit surface area [99]. Then, we find from Eqs. (58) and (60) that the monolayer of graphene embedded in the matrix of low-density polyethylene undergoes periodic static bending deformation (modulation) with the wavelength $\lambda_0 \approx 48.4$ Å, triggered by the compressive strain in the matrix as small as $\epsilon_{xx} = -2.5 \times 10^{-3}$. The bending modulation wavelength λ_0 is about 34 times larger than the carbon-carbon

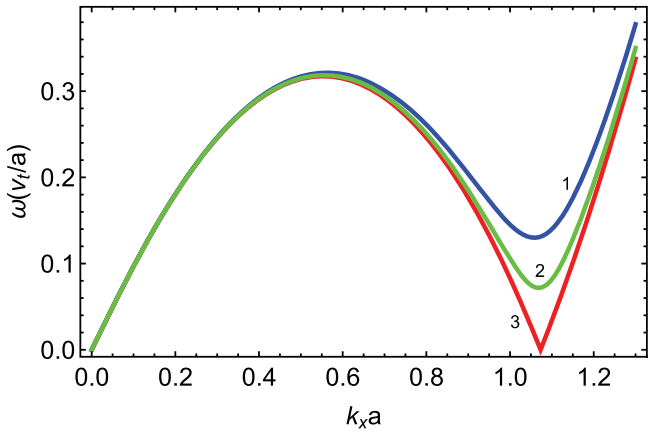

FIG. 15. Dispersion of flexural surface acoustic wave, propagating along the x axis in the graphene monolayer embedded in a matrix of low-density polyethylene, triggered by the compressive strain in the polyethylene along the x axis. Frequency is measured in units of v_t/a, wave vector k_x is measured in units of $1/a$, where $v_t = 0.466$ km/s, $a = \rho_s/\rho = 8.26$ Å for the polyethylene with density $\rho = 920$ kg/m^3. Lines 1, 2 and 3 correspond, respectively, to the strain $0.99\epsilon_{xx}^{(cr)}$, $0.997\epsilon_{xx}^{(cr)}$ and $1.0\epsilon_{xx}^{(cr)}$, where $\epsilon_{xx}^{(cr)} = -2.5 \times 10^{-3}$ is given by Eq. (60).

bond length $a^* = 1.42$ Å, that justifies the above description in the long-wavelength approximation. The bending modulation wavelength λ_0 is even larger in comparison with the effective *mechanical thickness* of graphene monolayer $d^* \approx 0.77$ Å, which can be found from the relation between bending stiffness D_s and Young modulus E_s of 2D elastic layer given by the theory of elasticity: $D_s = E_s d^{*2}/12$.

In Fig. 15 we present the change of the dispersion of surface acoustic waves, propagating along the x axis in the graphene monolayer embedded in soft matrix of low-density polyethylene, triggered by the compressive strain in the matrix along the x axis. Frequency is measured in units of v_t/a, the wave vector k_x is measured in units of $1/a$, where $v_t = 0.466$ km/s, $a = \rho_s/\rho = 8.26$ Å for the polyethylene with density $\rho = 920$ kg/m^3 [97]. Both the wave number of periodic bending deformation $k_{x0} = 1.07/a$ and the value of the negative surface stress g_{xx}, given by Eqs. (58) and (59), are very well confirmed by the numerical simulations. Close to the critical strain in the matrix $\epsilon_{xx}^{(cr)} = -2.5 \times 10^{-3}$, given by Eq. (60), the change of the dispersion around the wave number k_{x0} is very sharp: the lines 1, 2 and 3 correspond to the strain $0.99\epsilon_{xx}^{(cr)}$, $0.997\epsilon_{xx}^{(cr)}$ and $1.0\epsilon_{xx}^{(cr)}$, respectively. For $|\epsilon_{xx}| > |\epsilon_{xx}^{(cr)}|$, periodic static bending displacement of the graphene monolayer occurs, when $u_z^s = A\cos(k_{x0}x)$, with the amplitude $A = 2\sqrt{|\epsilon_{xx}| - |\epsilon_{xx}^{(cr)}|}/k_{x0}$ which can be found from the extremum of the functional, determined by the sum of the bending, in-plane membrane and surrounding matrix elastic energies of the monolayer embedded in the compliant matrix, for the given wave number k_{x0} and uniform surface stress $g_{xx} = g_{xx}^{(cr)} = E_s\epsilon_{xx}^{(cr)}$. The sharp cusp with $\omega = 0$, similar to the cusp shown by line 3 in Fig. 15, is present at the wave number $k_x = k_{x0}$ of the "condensation" of the flexural surface acoustic wave occurring in the embedded monolayer for $|\epsilon_{xx}| \geqslant |\epsilon_{xx}^{(cr)}|$. Similar sharp cusp with $\omega = 0$ is present at the corresponding wave number $k_x = k_{x0}$ of the "condensation" of the Rayleigh surface acoustic wave, which is produced by the statically modulated (periodically wrinkled) graphene monolayer bonded to the compressively strained compliant substrate and which occurs for $|\epsilon_{xx}| \geqslant |\epsilon_{xx}^{(cr)}|$. It is worth noting that such small value of the compressive strain $\epsilon_{xx}^{(cr)}$, critical for the occurrence of periodic static bending deformation, shows that even small local strains in the matrix (or in the substrate) can produce ripples in the supported graphene, similar to the ripples in suspended graphene [100,101].

VI. EFFECT OF NONLINEARITY ON TWO-PATH PHONON INTERFERENCE

It could be anticipated that nonlinear interactions between impurities results in higher harmonics which weaken the two-path interference and prevent the transmission coefficient from vanishing at the antiresonance. In this section, we study the effect of nonlinearity on the transmission interference antiresonance by analyzing the inelastic scattering of phonon wave packet in time domain. To this end, the generalized discrete nonlinear model is used which accounts for the local nonlinear interactions between impurities via an additional term U_{ah} in the lattice Hamiltonian, given by Eqs. (1)–(4):

$$U_{ah} = \sum_{m=1}^{4} \sum_{n_1,n_2} U_{n_1n_2}^{ah(m)}, \tag{61}$$

where

$$\begin{aligned} U_{n_1n_2}^{ah(1)} &= \frac{\zeta_1}{3} \sum_{\delta_i} \left(u_{2n_1}^{2n_2,0} - u_{2n_1+\delta_1}^{2n_2+\delta_2,\delta_3}\right)^3, \\ U_{n_1n_2}^{ah(2)} &= \frac{\nu_1}{4} \sum_{\delta_i} \left(u_{2n_1}^{2n_2,0} - u_{2n_1+\delta_1}^{2n_2+\delta_2,\delta_3}\right)^4, \\ U_{n_1n_2}^{ah(3)} &= \frac{\zeta_2}{3} \left(u_{2n_1+1}^{2n_2+1,1} - u_{2n_1+1}^{2n_2+1,-1}\right)^3, \\ U_{n_1n_2}^{ah(4)} &= \frac{\nu_2}{4} \left(u_{2n_1+1}^{2n_2+1,1} - u_{2n_1+1}^{2n_2+1,-1}\right)^4. \end{aligned} \tag{62}$$

The index δ_i here implies the summation over eight possible combinations of $\delta_1,\delta_2,\delta_3 = \pm 1$. The terms $U_{n_1n_2}^{ah(1)}$ and $U_{n_1n_2}^{ah(2)}$ characterize the cubic and quartic interaction between the impurities m_1, m_1^*, and m_2, respectively (see Fig. 1). The force constants ζ_1 and ν_1 are put alike for the impurities m_1 and m_1^*. The potential energies $U_{n_1n_2}^{ah(3)}$ and $U_{n_1n_2}^{ah(4)}$ with force constants ζ_2 and ν_2 describe the nonlinear interaction of the defect atoms with mass m_2 filling the plane $p_3 = -1$ with the defect atoms with mass m_2 filling the plane $p_3 = 1$.

We consider the propagation of the Gaussian phonon wave packet having the initial form

$$\begin{aligned} u_n &= Ae^{-(n-p_0)^2/\sigma^2} \sin(k_i n), \\ \dot{u}_n &= Ae^{-(n-p_0)^2/\sigma^2} \left[\frac{2v_g}{\sigma^2}(n-p_0)\sin(k_i n)\right. \\ &\quad \left. -\omega_i \cos(k_i n)\right], \quad n = n_3 = 1 \ldots N \end{aligned} \tag{63}$$

where the wave number k_i corresponds to the wave-packet central frequency $\omega_i = \omega_{\max}\sin(k_i/2) \approx \omega_R$, $v_g = \omega_{\max}\cos(k_i/2)/2$ is the group velocity of phonons with frequency ω_i, σ is the wave packet spatial width (coherence length) in units of lattice period, p_0 is a number of the plane where the displacement reaches maximum, the amplitude A

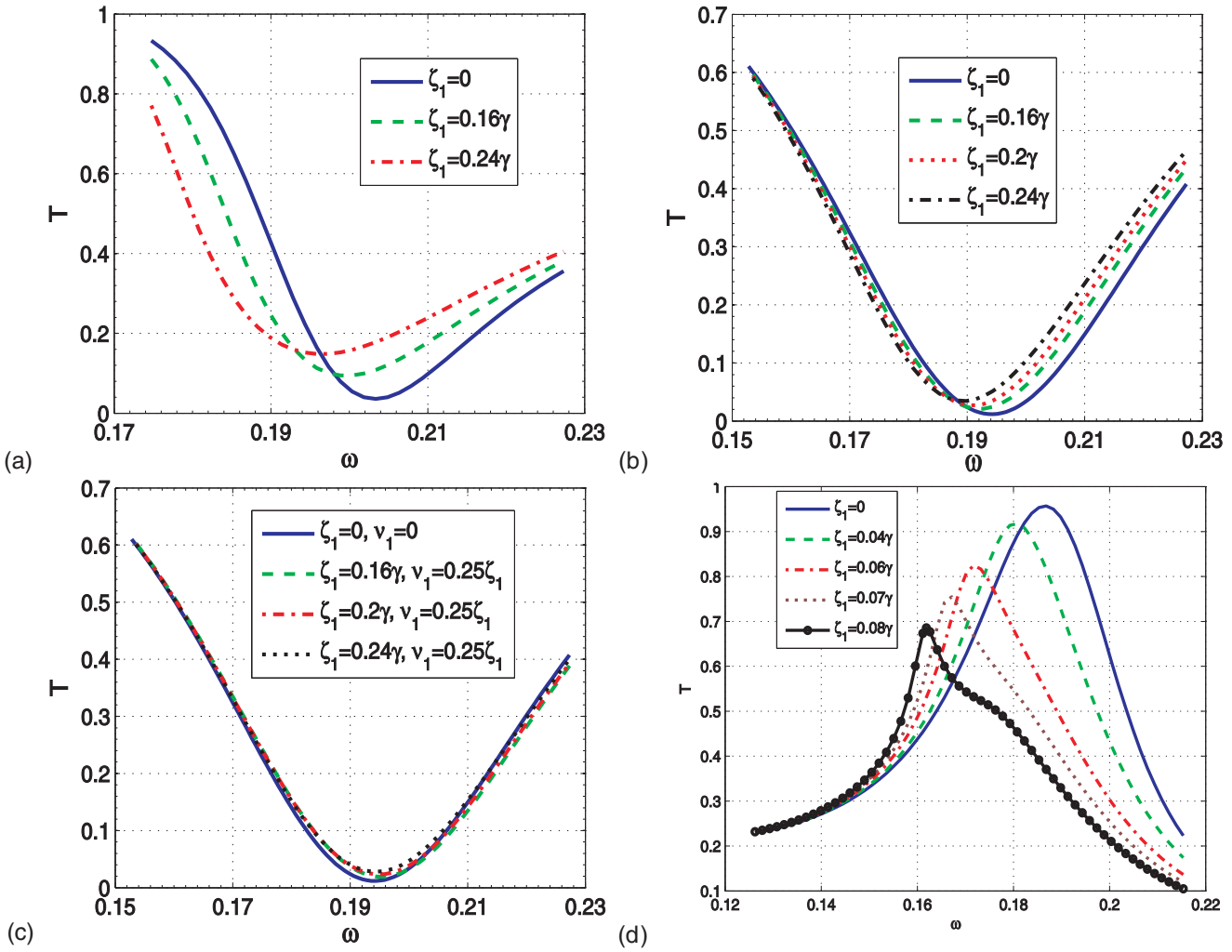

FIG. 16. Transmission coefficient of phonon wave packet with spatial width $\sigma = 120$ lattice periods versus reduced frequency in the nonlinear regime for the model, shown in Fig. 1, with $m_2 = m$, $\gamma_2 = \gamma$, $\gamma_3 = 0$, and with $m_1 = m_1^* = 2m$, $\gamma_1 = 0.14\gamma$, $\gamma_1^* = 0.6\gamma$ in (a), or with $m_1 = m_1^* = 2m$, $\gamma_1 = 0.14\gamma$, $\gamma_1^* = 1.8\gamma$ in (b) and (c), or with $m_1 = m_1^* = m$, $\gamma_1 = \gamma_1^* = 0.07\gamma$ in (d), for different values of cubic ζ_1 and quartic ν_1 anharmonic force constants.

is chosen such that in the input wave packet the maximum displacement is equal to 0.1. Thus, it is assumed that the Gaussian wave packet

$$u_n(t) = Ae^{-(n-p_0-v_g t)^2/\sigma^2} \sin(k_i n - \omega_i t) \qquad (64)$$

moves upwards normally to the defect planes (see Fig. 1).

We assume that our crystal is divided into identical layers composed of $N = 2^{12} = 4096$ parallel planes with the defect plane having the number $n = M + 2 = N/2 + 2$ (between the planes $n = M + 1 = N/2 + 1$ and $n = M + 3$). The nonlinear equations of motion are solved numerically with initial conditions (63) and periodic boundary conditions in vertical direction. We take $\sigma = 120$ and $p_0 = 1748$. The time interval of the wave-packet motion is $t_f = 900$. At the final time point t_f, the transmitted phonon energy is measured above the defect layer, at $n > M + 3$, and the reflected signal is measured below the layer, at $n < M + 1$.

Energy transmission and reflection coefficients at the wave-packet central frequency ω_i (or wave number k_i) are defined as

$$T = \frac{E_{tr}}{E_{\rm inc}}, \quad R = \frac{E_r}{E_{\rm inc}}, \qquad (65)$$

where $E_{\rm inc}$ is the total potential energy of the input pulse [see Eqs. (3), (4), (63), and (64)], E_{tr} and E_r are the total potential energies of the transmitted and reflected pulses, respectively, at $t = t_f$. Note that the energy conservation law holds fairly precisely in our simulations: the ratio $(E_{tr} + E_r)/E_{\rm inc}$ differs from 1 in the fourth digit only.

To study the effect of nonlinearity on the phonon-interference transmission antiresonaces, we fix the harmonic force constants and the amplitude A in the incident wave packet (such that in the input wave packet the maximum displacement is equal to 0.1) and compute the frequency dependencies of the transformation coefficients for different values of the local cubic and quartic anharmonic force constants. We found that the considered nonlinearities do not not remove the transmission minimum at the antiresonance (see also Refs. [74,75]). The transmission minimum can be slightly shifted around its value ω_R in the harmonic lattice, but its depth and spectral width remains practically the same, although the considered nonlinearities are fairly strong. The examples depicted in Fig. 16 illustrate this effect. (The symbol ω stands for the reduced frequency $\omega/\omega_{\rm max}$ in all the panels

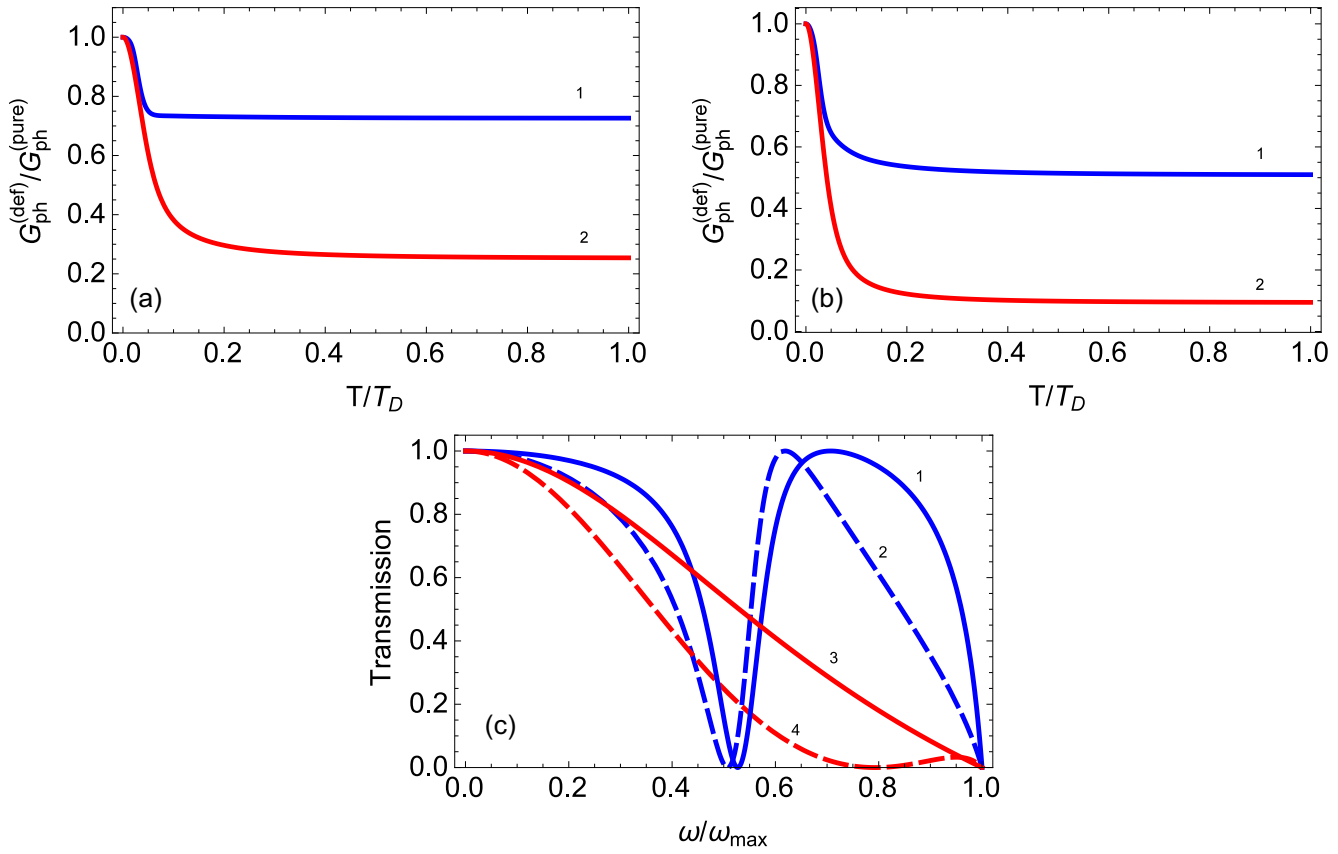

FIG. 17. Ratio of thermal conductances versus temperature, normalized by the effective Debye temperature, of 3D lattice of Si-like atoms with and without a defect plane half-filled in the chessboard order (lines 1) and fully filled (lines 2) with Ge-like atoms: (a) without ($\gamma_3 = 0$) and (b) with $\gamma_3 = 0.88\gamma$ non-nearest-neighbor coupling through the defect crystal plane (see Fig. 1). (c) Shows energy transmission coefficients versus reduced frequency through the defect plane in the lattice of Si-like atoms half-filled in the chessboard order (lines 1 and 2) or fully filled (lines 3 and 4) with Ge-like atoms, respectively, without, solid lines 1 and 3, and with, dashed lines 2 and 4, the next-to-nearest-neighbor coupling through the defect crystal plane $\gamma_3 = 0.88\gamma$.

in Fig. 16.) Figure 16(a) shows the observable shift of the antiresonance towards lower frequency governed by the local *cubic* anharmonic force constant, which in general *decreases* the eigenfrequency of anharmonic oscillator (the red shift) [102]. Figure 16(b) shows that the red shift of the antiresonace is reduced by the relative increase of the harmonic with respect to anharmonic defect-host force constants [cf. with Fig. 16(a)]. Figure 16(c) shows that the local *positive quartic* anharmonic force constant, which in general *increases* the eigenfrequency of anharmonic oscillator (the blue shift) [102], can counterbalance the red shift produced by the local cubic anharmonicity.

One more example illustrates the effect of nonlinearity on resonance transmission. We consider a crystal with the weakly bound planar defect in the FF model with $m_1 = m_1^* = m_2 = m$, $\gamma_1 = \gamma_1^* = 0.07\gamma$, $\gamma_2 = \gamma$, $\gamma_3 = 0$, in which there is a resonance of total transmission for the phonon plane wave with the frequency $\omega_T \approx 0.19\omega_{\max}$, given by Eq. (49), but there is no transmission antiresonance. Taking into account the local cubic anharmonicity in the system and launching the phonon wave packet with spatial width $\sigma = 120$ lattice periods and central frequency close to ω_T, we find the transmission spectrum presented in Fig. 16(d). As one can see in Fig. 16(d), the local cubic anharmonicity results in a decrease of the frequency of the constructive-interference Fabry-Pérot–type transmission resonance but does not fully suppress it, as in the case of the destructive-interference antiresonances shown in Figs. 16(a) and 16(b).

VII. EFFECT OF TWO-PATH PHONON INTERFERENCE ON THERMAL INTERFACE CONDUCTANCE

With the use of the analytical model, we also compute the thermal conductance of the cubic lattice of Si-like atoms with the two-dimensional defect, which is fully filled or half-filled with Ge-like atoms. The Ge-like atoms are considered as heavy-isotope defects in the lattice of Si-like atoms, with mass ratio 2.59. We calculate the interface thermal conductance G by following the Landauer-type formalism (see, e.g., Ref. [34])

$$G = \sum_{\nu} \int \hbar\omega_\nu v_{g\nu,z} \alpha\left(\omega_\nu, \frac{\mathbf{k}_\parallel}{\omega_\nu}\right) \frac{\partial}{\partial T} n_{\mathrm{BE}}(\omega_\nu, T) \frac{dk_z d^2\mathbf{k}_\parallel}{(2\pi)^3}$$
$$= \sum_{\nu} \int \hbar\omega_\nu^3 \alpha\left(\omega_\nu, \frac{\mathbf{k}_\parallel}{\omega_\nu}\right) \frac{\partial}{\partial T} n_{\mathrm{BE}}(\omega_\nu, T) \frac{d\omega_\nu}{(2\pi)^3} d^2\left(\frac{\mathbf{k}_\parallel}{\omega_\nu}\right), \quad (66)$$

where $\alpha(\omega_\nu,\mathbf{k}_\parallel/\omega_\nu)$ is energy transmission coefficient through the defect crystal plane of the phonon plane wave with frequency ω_ν and parallel to the interface wave vector $\mathbf{k}_\parallel$, where $\mathbf{k}_\parallel/\omega_\nu$ is determined by the incidence angle, $v_{g\nu,z} = \partial\omega_\nu/\partial k_z$ is the phonon group velocity in the normal to the interface direction, and $n_{\rm BE}(\omega,T) = [\exp(\hbar\omega/k_BT) - 1]^{-1}$ is the Bose-Einstein distribution of phonons at temperature T. (In this section, we use the notation α for the transmission coefficient, instead of notation T in previous sections, not to confuse it with the notation for temperature T.) The integration is carried out over the whole Brillouin zone of the lattice and the sum is taken over all the acoustic phonon branches $\nu = 1,2,3$. In Figs. 17(a) and 17(b), we plot the ratios between the thermal conductances of the lattice with the defect and of the pristine lattice, for the planar defects fully filled or half-filled, in the chessboard order, with heavy-isotope defect atoms, with mass ratio 2.59. Being mainly interested in the phonon interference effects, in the computed thermal conductance ratios we used the same form of the transmission spectra [see Fig. 17(c)] for the longitudinal and (two) transverse waves with the scaling factor 2 in frequency axis and neglected the incidence-angle dependencies of the transmission coefficients but took into account the three dimensionality of the system, which is preserved by the ω_ν^3 term in the integrand in Eq. (66). Temperature of the lattice is normalized by the effective Debye temperature: $T_D = \hbar\omega_{\rm max}/k_B$, where $\omega_{\rm max}$ is maximal frequency of longitudinal acoustic phonons in the lattice. As one can see in Fig. 17(b), a single planar defect of atomic-scale thickness in the lattice of Si-like atoms can reduce the thermal interface conductance by 50% in the case of half-filling and by 90% in the case of complete filling with Ge-like (heavy-isotope-defect) atoms with relatively weak non-nearest-neighbor coupling, $\gamma_3 = 0.88\gamma$, through the defect crystal plane (see Fig. 1). The comparison of Figs. 17(a) and 17(b) also shows that, counterintuitively, the additional next-to-nearest-neighbor coupling through the defect crystal plane with heavy-isotope defect atoms substantially decreases the interface thermal conductance (see also Refs. [66,72,74,75,77]). This effect demonstrates another possibility for the control of the lattice-wave heat transport by the two-path destructive phonon interference: more heat flux is impeded despite the opening of additional phonon paths. It is also important to emphasize that the reduction of the thermal interface conductance is larger in the three-dimensional lattice than in the quasi-1D chain, studied previously in Ref. [77], because of higher density of phonon states in the high-frequency domain in the 3D system, in which the transmission is most strongly suppressed by the additional phonon paths. Figure 17(c) shows the change of the transmission coefficients through the defect plane in the lattice of Si-like atoms half-filled in the chessboard order or fully filled with Ge-like atoms, induced by relatively weak non-nearest-neighbor coupling, $\gamma_3 = 0.88\gamma$, through the defect crystal plane. As one can see in Fig. 17(c), the non-nearest-neighbor coupling through the defect crystal plane indeed suppresses most strongly the transmission in the high-frequency domain. The ratio of the next-to-nearest- and nearest-neighbor force constants under the discussion, $\gamma_3/\gamma = 0.88$, we can compare with corresponding force constants ratio for Si crystal that can be found from the Tersoff potential [103], which is more than unit and is higher than that used in the plots in Figs. 17(b) and 17(c). In connection with the discussion of the next-to-nearest-neighbor force constants across the defect plane, we note that the introduction of the three-body Keating-type potentials between the atoms with mass m_2 through the atom with mass m_1 or through the atom with mass m_1^* shown in Fig. 1, which depend on the angles between interatomic bonds [104,105], results in the appearance of the effective next-to-nearest-neighbor pair potential between the atoms with mass m_2 across the defect plane. Such three-body interatomic potentials also produce interference transmission antiresonances at the defect crystal plane, which will be described elsewhere.

VIII. CONCLUSIONS

We have developed an analytical theory of the effects of interference in the two and more phonon paths on the transmission through and anomalous absorption in the impurity layers of atomic-scale thicknesses (2D defects), embedded in 3D crystal. The case of the 2D defects, fully or partially filled with weakly bound or heavy-isotope defect atoms, is considered taking also into account the long-range interatomic bonds. Our analysis covers different systems exhibiting the anomalous phonon transmission, reflection, and absorption features not present in the systems with only one-path phonon propagation. It is shown that a crystal plane, fully or partially filled with the impurity atoms, can become the strong obstacle for bulk phonons, which possesses one or several, depending on the number of *different phonon paths*, transmission dips (transmission antiresonances). The latter means that defect layers of atomic-scale thicknesses within certain frequency ranges are able to operate as perfect phonon metamirrors or meta-absorbers in realistic 3D crystal structures. Due to the cooperative superradiant effect, the spectral widths of the two-path interference antiresonances for the plane waves are determined by the square of the impurity surface density or partial filling fraction in the defect crystal plane.

We have considered the *anomalous interface absorption* with the total nontransmission and nonreflection of the incident phonon at the double-resonant defect monolayer with two equal frequencies of the local eigenmodes and two phonon paths through the defect plane. One of the results is the prediction of the *extraordinary phonon transmission* induced by the two-path constructive interference of lattice waves interacting with resonance oscillations of rare host atoms, periodically distributed in the crystal plane almost fully filled with heavy isotopes.

It is shown that the *phonon-interference-induced transparency* can be produced by the defect monolayer with the non-nearest-neighbor interactions, filled with two types of isotopes with relatively small difference in masses or binding force constants. In this case, a narrow transmission peak close to the antiresonance frequency accompanies a relatively broad transmission antiresonance.

We have analytically investigated the change from the total transmission to total reflection of the grazing-incident waves at the embedded monolayer defect as well as the anomalous resonance surface absorption. In the latter case, 50% of the energy of the oblique-incident long acoustic wave

is absorbed at the monolayer defect. In addition, it has been found that the softening of the flexural surface acoustic wave localized at the monolayer defect plane can occur due to negative (compressive) surface stress g_{xx} and finite bending stiffness of the embedded elastic nanolayer. Softening of the flexural surface acoustic wave results in spatially periodic static bending deformation (modulation) of the embedded nanolayer with the definite wave number k_{x0}. This effect can be induced by the compression of the matrix along the x axis, which results in the negative surface stress g_{xx} in the embedded 2D elastic layer. We estimate the necessary compressive strain ϵ_{xx} of the matrix and the resulting modulation wavelength $\lambda_0 = 2\pi/k_{x0}$ for the *graphene monolayer*, embedded in a strained matrix of low-density polyethylene: $\epsilon_{xx} = -2.5 \times 10^{-3}$, $\lambda_0 = 48$ Å.

We have analyzed the effect of nonlinearity on the one- and two-path phonon interference and show that the interference transmission antiresonances and resonances are shifted in frequencies but are not fully suppressed by rather strong anharmonicity of interatomic bonds. Destructive phonon interference in a defect monolayer reduces the Kapitza thermal interface conductance. Counterintuitively, an additional relatively weak non-nearest-neighbor coupling through the crystal plane filled with heavy-isotope defect atoms substantially reduces the thermal interface conductance and this effect is more pronounced in 3D system than in the quasi-1D systems, studied previously. The effect gain is a result of higher density of phonon states in the high-frequency domain in the 3D system, in which the transmission is most strongly suppressed by the additional phonon paths.

ACKNOWLEDGMENTS

Yu.A.K. thanks A. A. Berlin, A. Cantarero, O. V. Gendelman, H. Han, B. Li, L. I. Manevitch, M. A. Mazo, J. Ordonez-Miranda, A. A. Popov, K. Sääskilahti, T. Shiga, J. Shiomi, E. S. Syrkin, S. Volz, and S. Xiong for helpful discussions of several aspects of this work. The work of Yu.A.K. and I.A.S. was supported by the Russian Science Foundation in the part of the study of periodic bending deformation of graphene monolayer embedded in strained polyethylene (Grant No. 16-13-10302). The work of Yu.A.K. and I.A.S. was supported by the Federal Agency of Scientific Organizations of Russia in the part of the study of thermal interface conductance through two-dimensional defect layer (Research Topic 0082-2014-0013, No. AAAA-A17-117042510268-5). The work of A.N.D. was supported by the Federal Agency of Scientific Organizations of Russia in the part of the study of nonlinear interaction effect on multipath interference (Agreement No. 007-GZ/Ch3363/26). A.N.D. thanks the Ministry of Education and Science of the Russian Federation for financial support in the framework of Increase Competitiveness Program of NUST "MISiS" (Project No. K2-2017-079).

[1] P. L. Kapitza, The study of heat transfer in helium II, Zh. Eksp. Teor. Fiz. **11**, 1 (1941) [J. Phys. (USSR) **4**, 181 (1941)].

[2] E. T. Swartz and R. O. Pohl, Thermal boundary resistance, Rev. Mod. Phys. **61**, 605 (1989).

[3] G. Chen, *Nanoscale Energy Transport and Conversion: A Parallel Treatment of Electrons, Molecules, Phonons, and Photons* (Oxford University Press, Oxford, 2005).

[4] Z. Zhang, *Nano/Microscale Heat Transfer* (McGraw-Hill, NY, 2007).

[5] S. Volz, R. Carminati, P. Chantrenne, S. Dilhaire, S. Gomez, N. Trannoy, and G. Tessier, *Microscale and Nanoscale Heat Transfer* (Springer, Berlin, 2007).

[6] E. S. Toberer, L. L. Baranowski, and C. Dames, Advances in thermal conductivity, Annu. Rev. Mater. Res. **42**, 179 (2012).

[7] D. G. Cahill, W. K. Ford, K. E. Goodson, G. D. Mahan, A. Majumdar, H. J. Maris, R. Merlin, and S. R. Phillpot, Nanoscale thermal transport, J. Appl. Phys. **93**, 793 (2003).

[8] D. G. Cahill, P. V. Braun, G. Chen, D. R. Clarke, S. Fan, K. E. Goodson, P. Keblinski, W. P. King, G. D. Mahan, A. Majumdar *et al.*, Nanoscale thermal transport. II. 2003-2012, Appl. Phys. Rev. **1**, 011305 (2014).

[9] P. Hyldgaard and G. D. Mahan, Phonon superlattice transport, Phys. Rev. B **56**, 10754 (1997).

[10] M. V. Simkin and G. D. Mahan, Minimum Thermal Conductivity of Superlattices, Phys. Rev. Lett. **84**, 927 (2000).

[11] G. Chen, Thermal conductivity and ballistic-phonon transport in the cross-plane direction of superlattices, Phys. Rev B **57**, 14958 (1998).

[12] G. D. Mahan, Thermal transport in AB superlattices, Phys. Rev. B **83**, 125313 (2011).

[13] K.-H. Lin and A. Strachan, Thermal transport in SiGe superlattice thin films and nanowires: Effects of specimen and periodic lengths, Phys. Rev. B **87**, 115302 (2013).

[14] J. Garg and G. Chen, Minimum thermal conductivity in superlattices: A first-principles formalism, Phys. Rev. B **87**, 140302(R) (2013).

[15] R. Prasher, Predicting the thermal resistance of nanosized constrictions, Nano Lett. **5**, 2155 (2005).

[16] Y. Chalopin, J.-N. Gillet, and S. Volz, Predominance of thermal contact resistance in a silicon nanowire on a planar substrate, Phys. Rev. B **77**, 233309 (2008).

[17] M. Maldovan, Sound and heat revolutions in phononics, Nature (London) **503**, 209 (2013).

[18] B. C. Daly, H. J. Maris, K. Imamura, and S. Tamura, Molecular dynamics calculation of the thermal conductivity of superlattices, Phys. Rev. B **66**, 024301 (2002).

[19] P. K. Schelling, S. R. Phillpot, and P. Keblinski, Phonon wave-packet dynamics at semiconductor interfaces by molecular-dynamics simulation, Appl. Phys. Lett. **80**, 2484 (2002).

[20] B. C. Daly, H. J. Maris, Y. Tanaka, and S. Tamura, Molecular dynamics calculation of the in-plane thermal conductivity of superlattices, Phys. Rev. B **67**, 033308 (2003).

[21] Y. Chen, D. Li, J. R. Lukes, Z. Ni, and M. Chen, Minimum superlattice thermal conductivity from molecular dynamics, Phys. Rev. B **72**, 174302 (2005).

[22] S.-F. Ren, W. Cheng, and G. Chen, Lattice dynamics investigations of phonon thermal conductivity of Si/Ge superlattices with rough interfaces, J. Appl. Phys. **100**, 103505 (2006).

[23] E. S. Landry and A. J. H. McGaughey, Effect of interfacial species mixing on phonon transport in semiconductor superlattices, Phys. Rev. B **79**, 075316 (2009).

[24] K. Termentzidis, P. Chantrenne, and P. Keblinski, Nonequilibrium molecular dynamics simulation of the in-plane thermal conductivity of superlattices with rough interfaces, Phys. Rev. B **79**, 214307 (2009).

[25] L. Hu, L. Zhang, M. Hu, J.-S. Wang, B. Li, and P. Keblinski, Phonon interference at self-assembled monolayer interfaces: Molecular dynamics simulations, Phys. Rev. B **81**, 235427 (2010).

[26] Y. Chalopin, K. Esfarjani, A. Henry, S. Volz, and G. Chen, Thermal interface conductance in Si/Ge superlattices by equilibrium molecular dynamics, Phys. Rev. B **85**, 195302 (2012).

[27] K. Termentzidis, T. Barreteau, Y. Ni, S. Merabia, X. Zianni, Y. Chalopin, P. Chantrenne, and S. Volz, Modulated SiC nanowires: Molecular dynamics study of their thermal properties, Phys. Rev. B **87**, 125410 (2013).

[28] S. Merabia and K. Termentzidis, Thermal boundary conductance across rough interfaces probed by molecular dynamics, Phys. Rev. B **89**, 054309 (2014).

[29] Z. Liang and P. Keblinski, Finite-size effects on molecular dynamics interfacial thermal-resistance predictions, Phys. Rev. B **90**, 075411 (2014).

[30] Y. Chalopin, A. Rajabpour, H. Han, Y. Ni, and S. Volz, Equilibrium molecular dynamics simulations on interfacial phonon transport, Annu. Rev. Heat Transfer **17**, 147 (2014).

[31] J.-S. Wang, J. Wang, and N. Zeng, Nonequilibrium Green's function approach to mesoscopic thermal transport, Phys. Rev. B **74**, 033408 (2006).

[32] J.-S. Wang, N. Zeng, J. Wang, and Ch. Kwan, Nonequilibrium Green's function method for thermal transport in junctions, Phys. Rev. E **75**, 061128 (2007).

[33] I. M. Khalatnikov, Heat exchange between a solid and helium-II, Zh. Eksp. Teor. Fiz. **22**, 687 (1952) [Sov. Phys.–JETP **22**, 687 (1952)].

[34] I. M. Khalatnikov, *An Introduction to the Theory of Superfluidity* (Benjamin, New York, 1965).

[35] W. A. Little, The transport of heat between dissimilar solids at low temperatures, Can. J. Phys. **37**, 334 (1959).

[36] J. D. N. Cheeke, H. Ettinger, and B. Hebral, Analysis of heat transfer between solids at low temperatures, Can. J. Phys. **54**, 1749 (1976).

[37] A. C. Anderson, The Kapitza thermal boundary resistance between two solids, in *Nonequilibrium Superconductivity, Phonons, and Kapitza Boundaries*, edited by K. E. Gray (Plenum, New York, 1981), p. 1.

[38] O. Weis, Phonon radiation across solid solid interfaces within the acoustic mismatch model, in *Nonequilibrium Phonons in Nonmetallic Crystals*, edited by W. Eisenmenger and A. A. Kaplyanskii (North-Holland, Amsterdam, 1986), p. 1.

[39] H. Maris, Phonon focusing, in *Nonequilibrium Phonons in Nonmetallic Crystals*, edited by W. Eisenmenger and A. A. Kaplyanskii (North-Holland, Amsterdam, 1986), p. 51.

[40] A. G. Every, Phonon focusing in reflection and transmission, Phys. Rev. B **45**, 5270 (1992).

[41] Yu. A. Kosevich, Van der Waals coupled surface waves in nonpiezoelectric crystals and thin films, Phys. Lett. A **155**, 295 (1991).

[42] R. Prasher, Acoustic mismatch model for thermal contact resistance of van der Waals contacts, Appl. Phys. Lett. **94**, 041905 (2009).

[43] M. E. Lumpkin, W. M. Saslow, and W. M. Visscher, One-dimensional Kapitza conductance: Comparison of the phonon mismatch theory with computer experiments, Phys. Rev. B **17**, 4295 (1978).

[44] Ch. Steinbrüchel, The scattering of phonons of arbitrary wavelength at a solid-solid interface: Model calculation and applications, Z. Phys. B **24**, 293 (1976).

[45] P. E. Hopkins and J. R. Serrano, Phonon localization and thermal rectification in asymmetric harmonic chains using a nonequilibrium Green's function formalism, Phys. Rev. B **80**, 201408(R) (2009).

[46] D. L. Nika, E. P. Pokatilov, A. A. Balandin, V. M. Fomin, A. Rastelli, and O. G. Schmidt, Reduction of lattice thermal conductivity in one-dimensional quantum-dot superlattices due to phonon filtering, Phys. Rev. B **84**, 165415 (2011).

[47] B. V. Paranjape, N. Arimitsu, and E. S. Krebes, Reflection and transmission of ultrasound from a planar interface, J. Appl. Phys. **61**, 888 (1987).

[48] D. A. Young and H. J. Maris, Lattice-dynamical calculation of the Kapitza resistance between fcc lattices, Phys. Rev. B **40**, 3685 (1989).

[49] S. Pettersson and G. D. Mahan, Theory of the thermal boundary resistance between dissimilar lattices, Phys. Rev. B **42**, 7386 (1990).

[50] R. J. Stoner and H. J. Maris, Kapitza conductance and heat flow between solids at temperatures from 50 to 300 K, Phys. Rev. B **48**, 16373 (1993).

[51] J. C. Duda, T. E. Beechem, J. L. Smoyer, P. M. Norris, and P. E. Hopkins, Role of dispersion on phononic thermal boundary conductance, J. Appl. Phys. **108**, 073515 (2010).

[52] J. C. Duda, J. L. Smoyer, P. M. Norris, and P. E. Hopkins, Extension of the diffuse mismatch model for thermal boundary conductance between isotropic and anisotropic materials, Appl. Phys. Lett. **95**, 031912 (2009).

[53] P. E. Hopkins, T. Beechem, J. C. Duda, K. Hattar, J. F. Ihlefeld, M. A. Rodriguez, and E. S. Piekos, Influence of anisotropy on thermal boundary conductance at solid interfaces, Phys. Rev. B **84**, 125408 (2011).

[54] P. E. Hopkins and P. M. Norris, Effects of joint vibrational states on termal boundary conductance, Nanoscale Microscale Thermophys. Eng. **11**, 247 (2007).

[55] P. E. Hopkins, L. M. Phinney, J. R. Serrano, and T. E. Beechem, Effects of surface roughness and oxide layer on the thermal boundary conductance at aluminum/silicon interfaces, Phys. Rev. B **82**, 085307 (2010).

[56] A. J. C. Ladd, B. Moran, and W. G. Hoover, Lattice thermal conductivity: A comparison of molecular dynamics and anharmonic lattice dynamics, Phys. Rev. B **34**, 5058 (1986).

[57] K. Sääskilahti, J. Oksanen, J. Tulkki, and S. Volz, Role of anharmonic phonon scattering in the spectrally decomposed thermal conductance at planar interfaces, Phys. Rev. B **90**, 134312 (2014).

[58] Yu. A. Kosevich, Fluctuation subharmonic and multiharmonic phonon transmission and Kapitza conductance between crystals with very different vibrational spectra, Phys. Rev. B **52**, 1017 (1995).

[59] P. E. Hopkins, Multiple phonon processes contributing to inelastic scattering during thermal boundary conductance at solid interfaces, J. Appl. Phys. **106**, 013528 (2009).

[60] A. Feher, A. A. Mamalui, A. Ya. Dul'fan, E. S. Syrkin, and A. G. Shkorbatov, Low-temperature phonon transport in 3D point-contacts (Review), Low Temp. Phys. **31**, 921 (2005).

[61] Yu. A. Kosevich and E. S. Syrkin, Capillary phenomena and elastic waves localized near a plane crystal defect, Phys. Lett. A **122**, 178 (1987).

[62] Yu. A. Kosevich and E. S. Syrkin, Capillary phenomena and elastic vibrations near a plane defect in a crystal. I. Equations of boundary dynamics and properties of long surface waves, Kristallografiya **33**, 1339 (1988) [Sov. Phys.–Crystallogr. **33**, 797 (1988)].

[63] Yu. A. Kosevich and E. S. Syrkin, Capillary phenomena and elastic vibrations near a plane defect in a crystal. II. Instability of localized waves and formation of macroscopic deformational superlattice structures at a two-dimensional defect, Kristallografiya **33**, 1347 (1988) [Sov. Phys.–Crystallogr. **33**, 801 (1988)].

[64] Yu. A. Kosevich and E. S. Syrkin, Resonant interaction of elastic waves with a planar crystal defect, Fiz. Tverd. Tela (Leningrad) **33**, 2053 (1991) [Sov. Phys.–Solid State **33**, 1156 (1991)].

[65] Yu. A. Kosevich and E. S. Syrkin, Macroscopic dynamics of the interface between crystals and total resonance transmission of phonons, Fiz. Nizk. Temp. (Kharkov) **20**, 660 (1994) [Low Temp. Phys. **20**, 517 (1994)].

[66] Yu. A. Kosevich, Capillary phenomena and macroscopic dynamics of complex two-dimensional defects in crystals, Prog. Surf. Sci. **55**, 1 (1997).

[67] A. N. Darinskii and G. A. Maugin, The elastic wave resonance reflection from a thin solid layer in a crystal, Wave Motion **23**, 363 (1996).

[68] A. M. Kosevich and A. V. Tutov, Peculiarities of elastic wave scattering from a planar crystal defect and pseudosurface vibrations, Phys. Lett. A **248**, 271 (1998).

[69] Yu. A. Kosevich and E. S. Syrkin, Dissipative interaction and anomalous surface absorption of bulk phonons at a two-dimensional defect in a solid, Phys. Lett. A **251**, 378 (1999).

[70] Yu. A. Kosevich, E. S. Syrkin, D. A. Semagin, and A. M. Kosevich, Effect of Phonon Damping on the Resonance Reflection of a Transverse Sound Wave from a Planar Defect in a Crystal, Zh. Eksp. Teor. Fiz. **117**, 1122 (2000) [JETP **90**, 974 (2000)].

[71] A. M. Kosevich and V. I. Khokhlov, Singularities in the acoustic vibration spectrum of a crystal containing a planar defect, Fiz. Tverd. Tela (Leningrad) **10**, 56 (1968) [Sov. Phys.–Solid State **10**, 39 (1968)].

[72] Yu. A. Kosevich, Multichannel propagation and scattering of phonons and photons in low-dimensional nanostructures, Phys.-Usp. **51**, 848 (2008).

[73] Yu. A. Kosevich, A. Feher and E. S. Syrkin, Resonance absorption, reflection, transmission of phonons and heat transfer through interface between two solids, Low Temp. Phys. **34**, 575 (2008).

[74] H. Han, L. G. Potyomina, A. A. Darinskii, S. Volz, and Yu. A. Kosevich, Phonon interference and thermal conductance reduction in atomic-scale metamaterials, Phys. Rev. B **89**, 180301(R) (2014).

[75] Yu. A. Kosevich, H. Han, L. G. Potyomina, A. N. Darinskii, and S. Volz, Phonon interference and energy transport in nonlinear lattices with resonance defects, in *Quodons in Mica*, Springer Series in Materials Science 221, edited by J. F. R. Archilla (Springer, Switzerland, 2015), pp. 247–263.

[76] H. Han, B. Li, S. Volz, and Yu. A. Kosevich, Ultracompact Interference Phonon Nanocapacitor for Storage and Lasing of Coherent Terahertz Lattice Waves, Phys. Rev. Lett. **114**, 145501 (2015).

[77] H. Han, L. Feng, S. Xiong, T. Shiga, J. Shiomi, S. Volz, and Yu. A. Kosevich, Effects of phonon interference through long range interatomic bonds on thermal interface conductance, Low Temp. Phys. **42**, 711 (2016).

[78] C. K. Hong, Z. Y. Ou, and L. Mandel, Measurement of Subpicosecond Time Intervals Between Two Photons by Interference, Phys. Rev. Lett. **59**, 2044 (1987).

[79] C. Santori, D. Fattal, J. Vuckovic, G. S. Solomon, and Y. Yamamoto, Indistinguishable photons from a single-photon device, Nature (London) **419**, 594 (2002).

[80] J. Beugnon *et al.*, Quantum interference between two single photons emitted by independently trapped atoms, Nature (London) **440**, 779 (2006).

[81] C. Lang *et al.*, Correlations, indistinguishability and entanglement in Hong-Ou-Mandel experiments at microwave frequencies, Nat. Phys. **9**, 345 (2013).

[82] S. M. Wang *et al.*, Hong-Ou-Mandel interference mediated by the magnetic plasmon waves in a three-dimensional optical metamaterial, Opt. Express **20**, 5213 (2012).

[83] U. Fano, Effects of configuration interaction on intensities and phase shifts, Phys. Rev. **124**, 1866 (1961).

[84] N. W. Ashcroft and N. D. Mermin, *Solid State Physics* (Harcourt, Orlando, 1976).

[85] L. Verslegers, Z. Yu, Z. Ruan, P. B. Catrysse, and S. Fan, From Electromagnetically Induced Transparency to Superscattering with a Single Structure: A Coupled-Mode Theory for Doubly Resonant Structures, Phys. Rev. Lett. **108**, 083902 (2012).

[86] K. J. Boller, A. Imamoglu, and S. E. Harris, Observation of an Electromagnetically Induced Transparency, Phys. Rev. Lett. **66**, 2593 (1991).

[87] M. D. Lukin and A. Imamoglu, Controlling photons using electromagnetically induced transparency, Nature (London) **413**, 273 (2001).

[88] R. H. Dicke, Coherence in spontaneous radiation processes, Phys. Rev. **93**, 99 (1954).

[89] M. Gross and S. Haroche, Superradiance: An essay on the theory of collective spontaneous emission, Phys. Rep. **93**, 301 (1982).

[90] L. Feng, T. Shiga, H. Han, S. Ju, Yu. A. Kosevich, and J. Shiomi, Phonon-interference resonance effects by nanoparticles embedded in a matrix, Phys. Rev. B **96**, 220301(R) (2017).

[91] T. W. Ebbesen, H. J. Lezec, H. F. Ghaemi, T. Thio, and P. A. Wolff, Extraordinary optical transmission through subwavelength hole arrays, Nature (London) **391**, 667 (1998).

[92] F. J. Garcia-Vidal, L. Martin-Moreno, T. W. Ebbesen, and L. Kuipers, Light passing through subwavelength apertures, Rev. Mod. Phys. **82**, 729 (2010).

[93] A. F. Andreev and Yu. A. Kosevich, Capillary phenomena in the theory of elasticity, Zh. Eksp. Teor. Fiz. **81**, 1435 (1981) [Sov. Phys.–JETP **54**, 761 (1981)].

[94] H. J. Allen, *Analysis and Design of Structural Sandwich Panels* (Pergamon, Oxford, 1969).

[95] Yu. A. Kosevich and E. S. Syrkin, Anomalies of surface elastic waves and formation of superstructures as a result of two-dimensional deformation transitions, Fiz. Tverd. Tela (Leningrad) **29**, 3174 (1987) [Sov. Phys.–Solid State **29**, 1825 (1987)].

[96] Yu. A. Kosevich and E. S. Syrkin, Collective oscillations of twin boundaries in high-temperature superconductors as an acoustic analogue of two-dimensional plasmons, Phys. Rev. B **43**, 326 (1991).

[97] M. D. Lechner, Polymers, in *Springer Handbook of Condensed Matter and Materials Data*, edited by W. Martienssen and H. Warlimont (Springer, Berlin, 2005), p. 477.

[98] N. K. Balabaev, M. A. Mazo, A. V. Lyulin, and E. F. Oleinik, Plastic deformation of glassy polymethylene: Computer-aided molecular-dynamic simulation, Polymer Sci., Ser. A **52**, 633 (2010).

[99] T. J. Booth *et al.*, Macroscopic graphene membranes and their extraordinary stiffness, Nano Lett. **8**, 2442 (2008).

[100] J. C. Meyer, A. K. Geim, M. I. Katsnelson, K. S. Novoselov, T. J. Booth, and S. Roth, The structure of suspended graphene sheets, Nature (London) **446**, 60 (2007).

[101] A. Fasolino, J. H. Los, and M. I. Katsnelson, Intrinsic ripples in graphene, Nat. Mater **6**, 858 (2007).

[102] L. D. Landau and E. M. Lifshitz, *Mechanics* (Butterworth-Heinemann, Oxford, 2000).

[103] J. Tersoff, Empirical interatomic potential for silicon with improved elastic properties, Phys. Rev. B **38**, 9902 (1988).

[104] P. N. Keating, Effect of invariance requirements on the elastic strain energy of crystals with application to the diamond structure, Phys. Rev. **145**, 637 (1966).

[105] F. H. Stillinger and T. A. Weber, Computer simulation of local order in condensed phases of silicon, Phys. Rev. B **31**, 5262 (1985).